AN INVESTIGATION OF SURFACE AND INTERNAL WAVE-INDUCED TURBULENCE IN SHALLOW WATER THERMAL MICROSTRUCTURE

James Wesley Powell

NAVAL POSTGRADUATE SCHOOL
Monterey, California

THESIS

AN INVESTIGATION OF SURFACE AND INTERNAL
WAVE-INDUCED TURBULENCE IN
SHALLOW WATER THERMAL MICROSTRUCTURE

by

James Wesley Powell

Thesis Advisor: E. B. Thornton

March 1974

Approved for public release; distribution unlimited.

An Investigation of Surface and Internal Wave-Induced Turbulence in Shallow Water Thermal Microstructure

by

James Wesley Powell
Captain, Canadian Armed Forces
B.Sc., University of British Columbia, 1964

Submitted in partial fulfillment of the
requirements for the degree of

MASTER OF SCIENCE IN OCEANOGRAPHY

from the

NAVAL POSTGRADUATE SCHOOL
March 1974

ABSTRACT

Measurements of temperature, wave height, and orthogonal water particle velocity were made in May 1973 at the NUC Tower located one mile off Mission Beach, California. A detailed analysis of the temperature field was made using digital temperature and isotherm contour plots. Billow turbulence microstructure appeared to be the dominant mechanism with the exception of one run in which evidence of double-diffusion microstructure was found. Spatial correlation lengths, calculated from the plot of the covariances, were of the order of 130 cm and less when the signal was high-pass filtered for waves of 100 seconds and longer. No depth dependence was noticed. Both frequency and wavenumber spectra were calculated and a correspondence between the spectra was noted at the frequency and wavenumber of the surface wave-induced particle displacements.

The Thornton, Boston, Whittemore model of wave-induced temperature fluctuations was tested and found to model the temperature spectra quite well, especially in a narrow band of frequencies associated with surface waves. The turbulent temperature spectrum, calculated as the difference between the actual and wave-induced spectra, had a slope near -5/3 above 0.1 Hz and more negative at lower frequencies.

TABLE OF CONTENTS

LIST OF TABLES

LIST OF FIGURES

ACKNOWLEDGEMENTS

The author is greatly indebted to both Dr. E. Thornton and Dr. N. Boston for their time and effort in bringing this paper to fruition.

The research and experiment was funded under the following project:

ONR Project No. NR 083-275

I. INTRODUCTION

A. HISTORY

For the past three years research has been carried out at the United States Naval Postgraduate School (NPS), Department of Oceanography, to study the shallow water interactions that occur between various oceanographic parameters such as temperature, salinity, surface waves, internal waves, and sound speed. These experiments have been conducted from the Naval Undersea Research and Development Center's (NUC) Oceanographic Research Tower located approximately one mile off Mission Beach, California. Results of the experiments are presented in NPS Theses, NPS technical reports and publications. This thesis is based on a study started by Whittemore (1973) and is an extension of the results obtained by Minard (1973).

The Whittemore experiment was conducted at NUC on 8 and 9 June 1972. Measurements were made of salinity, sound velocity, particle velocity, and temperature (at various positions along a horizontal array) for ten preselected depths. He concluded that the relationship between temperature fluctuations and surface wave height (for swell type waves) was of the form,

$$T(t) = K(f,z) \cdot \frac{dT}{dz} \cdot \eta(t) \ ,$$

and that a similar relationship was likely to exist between temperature fluctuations and internal waves. He also found that turbulence degrades coherence between temperature fluctuations in sensors displaced spatially; however, a lack of temperature sensors prevented him from making definitive statements.

Reworking the data collected during the June 1972 experiment, Thornton (1974) demonstrated a means for separating turbulent and surface wave-induced vertical velocity spectral components allowing for the quantities to be statistically correlated. The method applied to the wave and velocity measurements allowed the wave energy density spectral components to be converted to velocity spectral components using linear wave theory. The computed values compared very well with the measured velocity spectra for the moderate wave conditions encountered and appeared to verify the theoretical spectral transfer function and assumed linear system.

Using the same data and techniques, Thornton, Boston, and Whittemore (1974) devised a means for separating turbulent and surface wave-induced temperature fluctuations. They assumed that linear wave theory could be used to describe the surface waves; that the temperature isotherms were horizontal; and that the mean temperature gradient was a constant. In this way they developed a stochastic model describing the surface wave-induced temperature fluctuations. This allowed a means for calculating the

turbulent temperature spectrum by subtracting out the wave-induced contributions. The measured slope of the turbulent temperature spectra closely approximated the Kolmogorov -5/3 slope over a decade. This supported the result that the turbulent temperature fluctuations are statistically independent of the surface wave-induced velocities.

In the present work it is intended to refine the analysis of the data and extend the results obtained by Minard (1973). Minard set out to rectify the lack of sensors noted in Whittemore's experiment and conducted another experiment at NUC on 15 and 16 May 1973. Measurements of small scale temperature fluctuations were made in 19 meters of water using a movable array of seven thermistors, with a short (0.015 sec) response time; and accurate to 0.01°C in seawater. A schematic of the tower and instrument mounting is given in Figure 1. In addition to temperature, wave heights and orthogonal water particle velocities were measured simultaneously. Measurements were made at various depths with either a vertical or horizontal orientation of the temperature array.

Minard found that in the presence of internal waves temporal scales were of the order of 4 seconds and spatial scales were of the order of 33 cm, whereas outside the influence of internal waves they were of the order of 10 seconds and 118 cm. It was concluded that in the presence

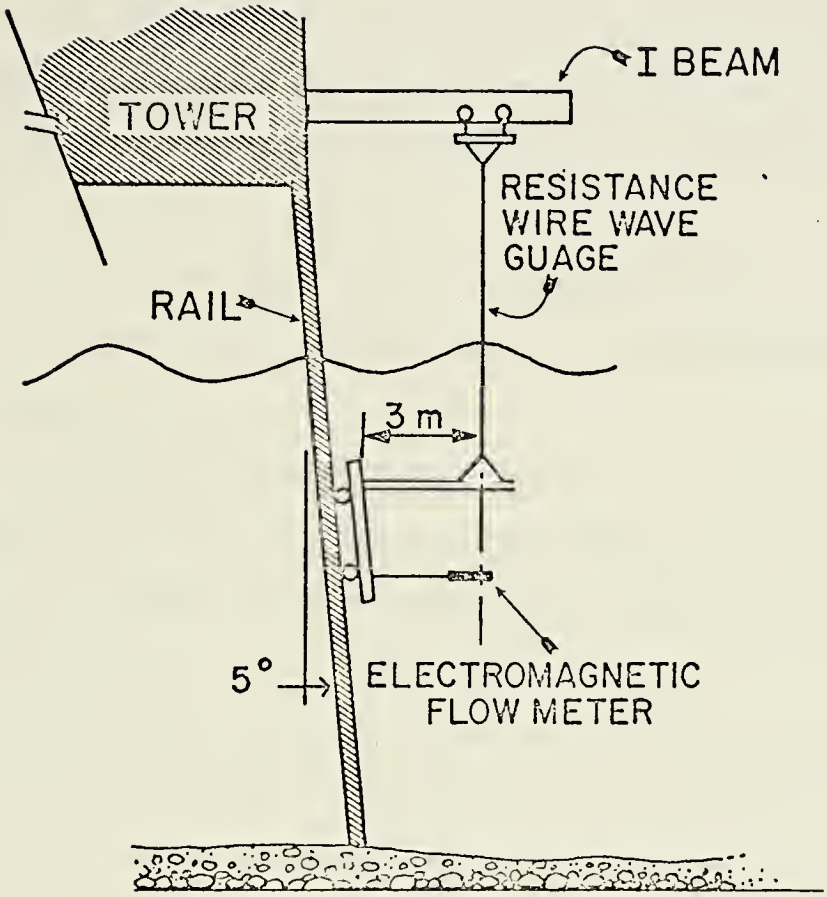

Figure 1. Schematic of Tower and Instrument Mounting.

of internal waves, correlation times were similar for both vertical and horizontal scales and spatial correlation lengths were similar for vertical and horizontal scales.

B. OBJECTIVES

The main objectives of this thesis with relation to the measurements made by Minard in May 1973 are to:

1. Define the spatial and temporal temperature field.

2. Define the spatial and temporal temperature spectra and determine if an obvious relationship exists between them.

3. Define the temperature gradient field and its variation with time to enable a comparison to be made between the formation of microstructure with and without the passage of an internal wave.

4. Test the stochastic model proposed by Thornton, Boston, and Whittemore to calculate the theoretical wave-induced temperature spectrum using these data.

II. THEORETICAL CONSIDERATIONS

The creation of small scale temperature fluctuations in shallow water is a complex process occurring at all depths and scales, depending on the operative driving function prevailing in time and space. In the near surface regime winds over the surface produce tangential surface stresses both from the interfacial stress and from the momentum loss associated with processes such as breaking waves. These result in a downwards momentum transfer with its attendant downward flux of heat and salt from the surface to a depth dependent on the stability of the water column, the gradient of shears produced, and the wavelength of the surface waves. In this way the temperature and salinity in the mixed layer become virtually uniform; and, unless the stability or Brunt-Väisälä frequency (defined as

$$N^2 = - \frac{g}{\rho} \frac{\partial \rho}{\partial z} , \qquad (1)$$

where g is the acceleration of gravity, ρ is the density and $\frac{\partial \rho}{\partial z}$ is gradient of density) is less than or equal to zero, a thermocline develops due to the increasing contrast between the properties of the water in and below the mixed layer. If there is substantial surface cooling, there may be a region below the mixed layer in which the

stability frequency is less than zero and convective motions can develop extending to considerable depth, particularly in polar waters (Phillips, 1969).

The ocean bottom exerts a retarding force on any near bottom water moving over it. The resulting shear zone again causes turbulent mixing. In the absence of dynamic instabilities leading to a complete overturn, the bottom turbulence will produce a mixed layer similar to that formed in the surface layer and consequently intensify the the thermocline from the bottom.

If a thermocline is formed, it will inhibit the vertical extent of mixing from either above or below depending on the depth of the thermocline and the intensity of the gradient within it. Turbulence produces changes which tend towards three-dimensional isotropy, and as such will be seriously inhibited by a constraint in any direction. In this case, the vertical motion is inhibited and results in a flow of energy out of the other two components of velocity in an effort to boost the vertical energy. Hence, an increase in stability as defined by an increased degree of stratification or density gradient may well be associated with the degradation of turbulence within the water column, and in particular, that associated with internal waves.

Paradoxically, the thermocline, which tends to inhibit turbulent mixing from the vertical boundaries, may itself

be a source of increased turbulence. Internal waves propagate along the thermocline and can lead to increased turbulence through shears developed between water masses either above or below the thermocline. In addition, under certain conditions the different rates of diffusion of heat and salt across the thermocline lead to a small scale perturbation in the temperature field.

For the purposes of this thesis, the scales to which turbulent temperature fluctuations may be broken down fall into three convenient, though not necessarily independent, classifications. These are: microstructure effects, surface wave effects, and internal wave effects. Each of these will be discussed separately.

A. MICROSTRUCTURE EFFECTS

Much evidence is now available which shows that vertical mixing in the interior of stable fluids occurs, on occasion, at scales much smaller than the vertical extent of the water column (Woods and Wiley, 1972). Although turbulence can enter at any boundary of a fluid, as long as vorticity is generated, two processes have been proposed as capable of producing intense vertical microstructure activity. The first arises from the differing rates of diffusion of heat and salt (double-diffusion or salt-fingering). The second process is turbulent mixing driven either by surface winds or by shear instabilities (billow turbulence). It occurs at the vertical

boundaries or on internal waves at depth.

1. Double-Diffusion and Salt-Fingering

This process is a local one operating where weak mixing has already increased the vertical gradients of temperature and salinity, and whose vertical scale seldom exceeds a few meters (Gregg, 1973). Considering only a two layer system involving both heat and salt gradients, three distinct situations can arise.

The first is an inherently stable system where the upper layer is both warmer and less saline than the lower layer. It is of less interest because both components act together to produce a stable density step across the interface.

The second situation is an inherently unstable system where the upper layer is both warmer and more saline than the lower layer. In a very few minutes there will be a rapid loss of heat in the upper layer making it more dense than the lower layer, which is simultaneously gaining heat and consequently becoming less dense. The result is alternate fingers of 'heavier' water sinking and 'lighter' water rising, hence its name - Salt-Fingering (Figure 2). The pattern of convection will persist only to a limited depth where the descending more saline water undergoes weak overturning to form a well mixed layer of temperature and salinity intermediate to the parent waters. In such a system a series of steps will form beneath the interface with steps of the order of

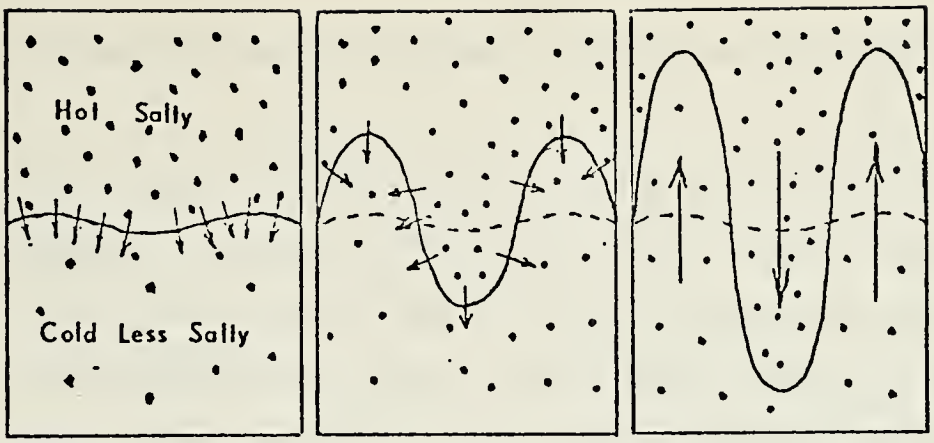

Figure 2. SALT-FINGERING- The solid lines show the initial and subsequent density profiles when the more rapid diffusion of heat has produced a potentially unstable situation at the interface. (From Gregg, 1973)

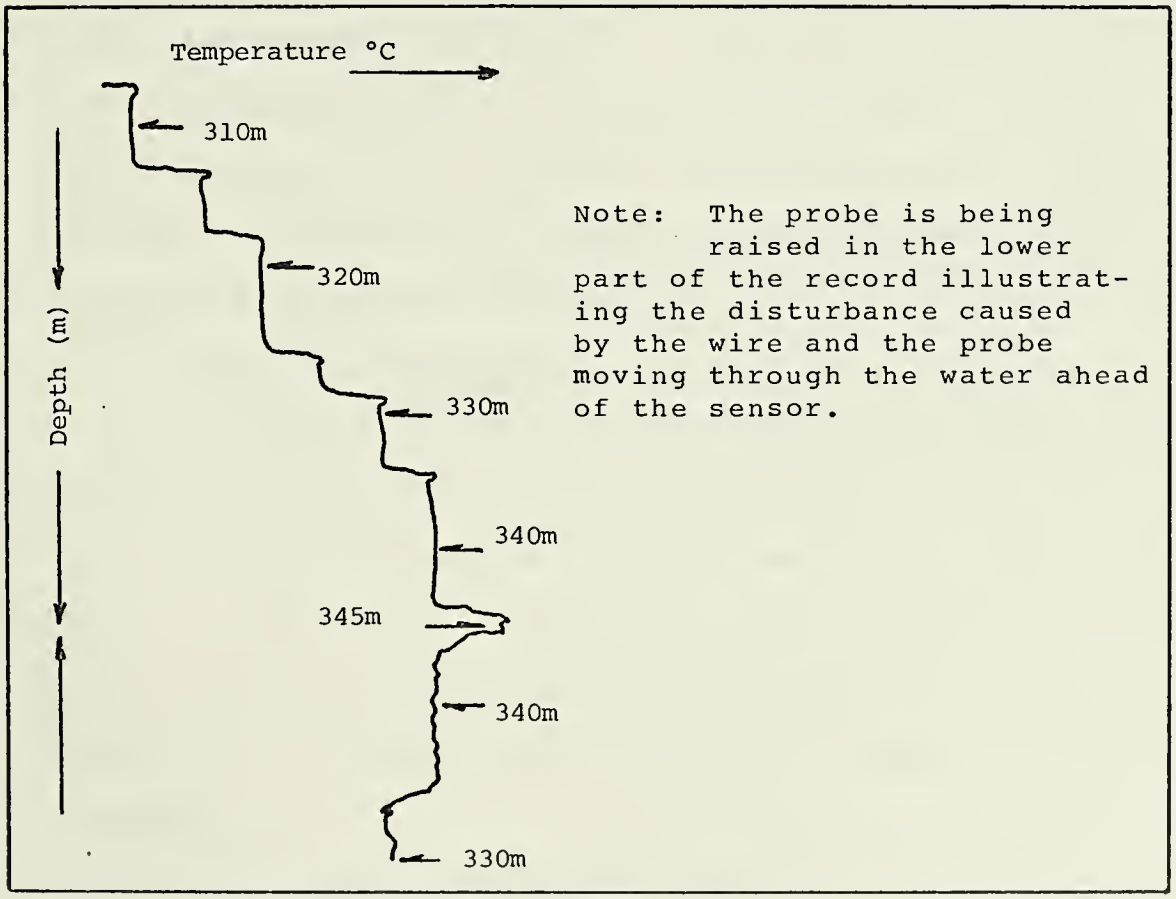

Figure 3. High resolution temperature profile of the 310-345m. interval in the Arctic off Ice-Island T-3 (From Denner, 1971).

20-30 centimeters and interfaces as small as two centimeters.

The third situation is one in which the layers remain separate but where convective mixing occurs within each. It is characterized by a cooler, less saline upper layer and a warmer, more saline lower layer. Again there is a rapid diffusion of heat across the interface but now it acts to increase the stability between the two layers with intense convective mixing within each of the layers. In a manner similar to that for salt-fingering the convection is self-limiting and extends into a series of steps above the original interface. Neshyba, Neal and Denner (1971) found as many as 40 steps above a layer of warm saline Atlantic water that had entered the Arctic. Each is about 3-10 meters per step and with interfaces of the order of centimeters (Figure 3).

2. Billow Turbulence

Billow turbulence is described as free shear turbulence modified by a density gradient and initiated by Kelvin-Helmholtz instability (Woods and Wiley, 1972) which is illustrated in Figure 4. This microstructure is very complex in form as opposed to the rather simple, symmetrical configuration of the density steps in double-diffusion.

It appears that a great majority of the flow within the thermocline is laminar and devoid of turbulent

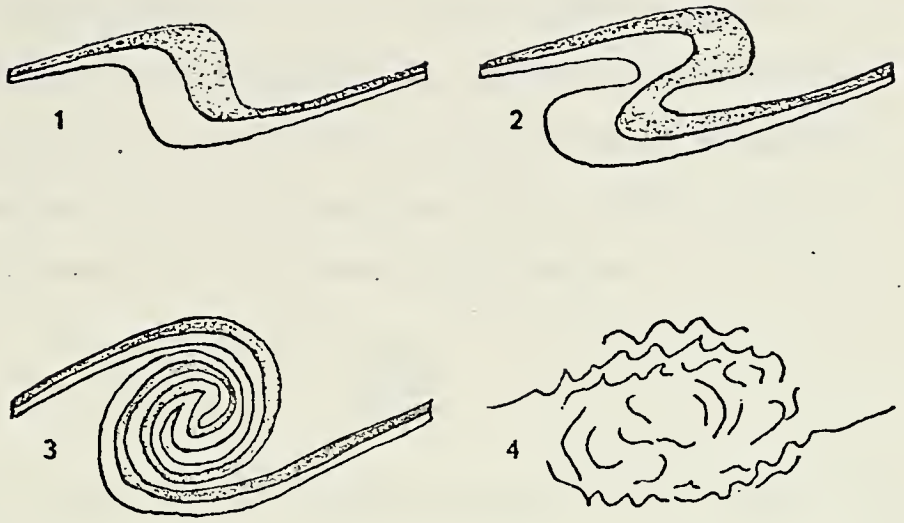

Figure 4. KELVIN-HELMHOLTZ SHEAR INSTABILITY
The upper layer has a higher velocity and a lower density than the lower layer. The instability, generated in a two-layer laboratory tank by rapidly raising and then lowering one end of the tank, caused the two layers to soon lose their coherence and break up into turbulent patches. The diagrams are based on a study by S. A. Thorpe of the National Institute of Oceanography in England. (From Gregg, 1973)

motions on any scale (Woods and Wiley, 1972). Occasionally, however, shear instability is triggered within small regions by boundary produced shears or internal gravity waves. In this latter case, as one of the wave packets travels along a sheet, shear instability is produced at the crests of sufficient height to cause the local Richardson's number of the billow to fall below a critical value of 0.25 (Woods and Wiley, 1972). The Richardson number for the sheet is given by

$$J = \frac{gh\Delta\rho}{\rho\Delta v^2}$$

where "g" is gravitational acceleration, "h" is the thickness of the shear zone, "$\Delta\rho/\rho$" is the fractional density difference, and "ΔV" is the velocity difference across the shear. For a given value of $J < 0.25$ the layer will be unstable to a specific range of wavelengths, of which $L_c = 7.5 \times h$, will be the fastest growing disturbance (Woods, 1968a).

The condition for termination of turbulent motions is that the Richardson number again increases above the critical value of 0.25 to about unity. When this is reached, the billow no longer extracts sufficient kinetic energy from the shear to supply the billow turbulence and the turbulent motions decay. Woods and Wiley (1972) found that in the sea the approximate scales were 75 cm for the billows, 500 cm for the patch of turbulence, and 300 sec

for the lifetime of the turbulence.

B. SURFACE WAVE EFFECTS

During the past few years considerable effort has been put into understanding the effects of wave motion on the thermocline but relatively little has been done to understand the internal temperature effects such waves produce. Clearly, temperature fluctuations in the near surface region can be caused by a number of factors, including surface waves and their associated turbulence, internal waves, and advection. Surface wave effects on temperature fluctuations are usually considered only to depths of less than one-half of one wavelength due to the exponential decay of particle motion with depth. However, the energy densities of surface wave-induced fluctuations are in the same frequency band and of the same order of magnitude when they are present simultaneously and hence are very difficult to separate. Therefore the spectral separation of the turbulent and wave-induced temperature fluctuations will be considered in greater detail later in this thesis.

The temperature field can be considered as a turbulent field having an "energy" containing region, an "inertial" subrange, and an "energy" dissipation region analogous to that hypothesized for velocity fields. In addition, since the rates of thermal and viscous dissipation are different in the ocean, the smaller scale temperature field will tend to persist longer than the velocity field.

1. Surface Wave-induced Temperature Fluctuations

Earlier, mention was made of a paper (Thornton et al, 1974) setting out a relationship between wave-induced temperature fluctuations and the waves. The major portion of what follows is taken directly from that paper and is included here, in a somewhat abbreviated form, for completeness.

Thornton (1974) had previously shown that linear wave theory estimated the wave-induced water particle motion very well under small amplitude wave conditions. Since it worked for particle motion, linear wave theory was assumed to estimate the wave-induced temperature fluctuations. This implies that the flow is irrotational. It was further assumed that the temperature fluctuations are small, allowing density to be considered constant over short distances. Hence, temperature is considered to be a passive scalar with buoyancy effects neglected. Assuming temperature is a conservative property, at least in the body of the flow, the conservation of temperature flux is given by

$$\frac{\partial \theta}{\partial t} + u_i \frac{\partial \theta}{\partial x_i} + v \frac{\partial \theta}{\partial z} = 0 \qquad (2)$$

where $\theta(x_i,z,t)$ is the measured temperature, $u_i(x_i,z,t)$ are the horizontal velocities, $v(x_i,z,t)$ is the vertical velocity, x_i are the horizontal cartesian coordinates, z is the vertical cartesian coordinate. The equation

considers the individual time change, advection, and diffusion of the passive scalar temperature. In terms of their means, turbulent fluctuations and wave-induced fluctuations the quantities are defined as

$$\theta = \bar{\theta} + \theta_w + \theta'$$

$$u_i = \bar{u}_i + (u_w)_i + u_i'$$

$$v = v_w + v'$$

where the overbar indicates a time-averaged mean, the subscript w indicates contributions from surface waves, and the prime indicates turbulent motions.

Assuming that

(1) turbulent and wave-induced motions are statistically independent,

(2) mean temperature isotherms are horizontal,

(3) mean velocities are zero, and

(4) the mean vertical temperature gradient is constant,

allows separation of the turbulent motions and Equation (2) reduces to

$$\frac{\partial \theta_w}{\partial t} + (u_w)_i \frac{\partial \theta_w}{\partial x_i} + v_w \frac{\partial}{\partial z} (\bar{\theta} + \theta_w) = 0 \qquad (3)$$

where the velocities and the assumption of irrotational flow are as specified in linear wave theory.

Temperature fluctuations caused by wave-induced velocities are a priori assumed equal to zero and

therefore

$$(u_w)_i \frac{\partial \theta_w}{\partial x_i} + V_w \frac{\partial \theta_w}{\partial z} = 0 \ .$$

This leaves a first order, constant coefficient, homogeneous differential equation, if the mean temperature gradient is constant, and therefore

$$\frac{d\theta_w}{dt} = - \frac{\partial \bar{\theta}}{\partial z} \ V_w \ . \qquad (4)$$

This is easily integrated to give

$$\theta_w(x_i,z,t) = [- \frac{\partial \bar{\theta}}{\partial z} \frac{\sinh k(d+z)}{\sinh kd}] \ a \cos (k_i x_i - \sigma_i t) \qquad (5)$$

where $V_w(x_i,z,t)$ is the wave-induced vertical water-particle velocity specified by linear wave theory, 'a' is the surface wave amplitude, k is the wave number, σ is the radian frequency, d is the depth, and z is the negative downwards displacement from the mean water surface.

In terms of the spectral transfer function, $H_\theta(\sigma)$ (the square bracket in Equation (5)), and the sinusoidal surface displacements, $\eta(x_i,t)$, Equation (5) reduces to

$$\theta_w(x_i,z,t) = H_\theta(\sigma) \ \eta(x_i,t) \qquad (6)$$

Equation (6) satisfies Equation (3) exactly, which means that moderate swell type waves do little or no mixing, but only serve to pump the thermocline up and down.

2. Turbulent Temperature Spectrum

In a manner similar to that discussed in Thornton, (1974) the paper by Thornton, Boston, and Whittemore (1974) discusses the separation of the turbulent temperature spectrum from the wave-induced temperature spectrum. For completeness the arguments are repeated here.

The wave-induced temperature spectrum, $S_{\theta_w}(\sigma)$, is calculated from the wave spectrum, $S_\eta(\sigma)$, using the complex transfer function, $H_\theta(\sigma)$ (given in Equation (6)), in the form

$$S_{\theta_w}(\sigma) = |H_\theta(\sigma)|^2 S_\eta(\sigma) \quad . \tag{7}$$

In terms of the total temperature spectrum the turbulent temperature spectrum is given by

$$S_{\theta'}(\sigma) = S_\theta(\sigma) + S_{\theta_w}(\sigma) - 2\mathrm{Re}\{H_\theta(\sigma) \cdot S_{\theta\eta}(\sigma)\} \quad . \tag{8}$$

If the cross-spectrum is expressed in terms of its co- and quadrature spectra

$$S_{\theta\eta}(\sigma) = C_{\theta\eta}(\sigma) + iQ_{\theta\eta}(\sigma)$$

then Equation (8) becomes

$$S_{\theta'}(\sigma) = S_\theta(\sigma) + S_{\theta_w}(\sigma) - 2H_\theta(\sigma)\, C_{\theta\eta}(\sigma) \tag{9}$$

which gives the turbulent temperature spectrum in terms of measurable quantities.

Assuming statistical independence between turbulent and wave-induced temperature leads to further simplification, since

$$S_{\theta_\eta}(\sigma) = S_{\theta_{w\eta}}(\sigma)$$

and

$$H_\theta(\sigma) S_{\theta_{w\eta}}(\sigma) = S_{\theta_w}(\sigma) = |H_\theta(\sigma)|^2 S_\eta(\sigma) .$$

This allows the turbulent temperature spectrum to be given simply as the actual temperature spectrum minus the wave-induced temperature spectrum, or,

$$S_{\theta'}(\sigma) = S_\theta(\sigma) - |H_\theta(\sigma)|^2 S_\eta(\sigma) . \qquad (10)$$

Further the coherence between temperature fluctuations and the waves is then given by

$$\gamma_{\theta_\eta}^2(\sigma) = \left[1 + \frac{S_{\theta'}(\sigma)}{S_{\theta_w}(\sigma)}\right]^{-1} = \frac{S_{\theta_w}(\sigma)}{S_\theta(\sigma)} . \qquad (11)$$

C. INTERNAL WAVE EFFECTS

Internal waves are subsurface waves existing between layers of different density or within layers where a vertical density gradient exists. They occur often due to a variety of causes such as flow over an irregular bottom, atmosphere disturbances, tidal forces, and shear flow.

The theory of the existence of internal waves implies perfect coherence of plane waves over space; whereas in practice naturally occurring internal waves are not so coherent. In addition, the ocean contains a number of generating sources which may reinforce or cancel each other (LaFond, 1966).

In shallow water, at the same site as this experiment, LaFond (1966) found internal waves of amplitudes ranging from 2 to 23 feet with mean amplitude of 5.6 feet. In general, the magnitude of the shorter period waves was found to be inversely proportional to the gradients in which they were found. Theoretically, internal waves have periods ranging between the lower inertial and higher Väisälä or stability frequencies. LaFond found periods ranging from 4 to 10 minutes superimposed on longer diurnal cycles and four and one-half day cycles. He also found that internal waves moving towards the shore had an average speed of 0.31 knots and ranged from 0.11 to 0.60 knots.

Physical intuition would lead us to suspect that temperature fluctuations associated with internal waves should exhibit a linear relationship between the temperature gradient and the wave amplitude. Therefore a reasonable expression for the temperature fluctuations associated with internal waves would be

$$\theta_{iw}(t) = \frac{\partial \bar{\theta}}{\partial z} \cdot A_o(t)$$

where the overbar indicates the time-averaged mean and $A_o(t)$ is the instantaneous amplitude of the internal wave.

The temperature fluctuations due to internal waves are usually easily identified because of the narrow range of frequencies where significant energy is present, and the presence of a valley, in the spectral energy density, separating the surface and internal wave regions. Further, energy contained in the turbulent temperature fluctuations is small relative to the energy of the internal waves, and is, therefore, only a minor feature at these low frequencies.

III. EXPERIMENT AND DATA ANALYSIS

A. EXPERIMENT

Measurements were made at various depths with either a vertical or horizontal orientation of the temperature array as summarized in Table I.

TABLE I. Summary of Experimental Set-up for Minard's May 1973 Experiment

Run Number	Date	Time	Depth to top of frame(m)	Array disposition	Internal waves	Digi-tized	Tide
1	15 May	1300	2.7	vertical	no	yes	ebb
2	15 May	1437	5.2	vertical	yes(1)	yes	slack
3	15 May	1607	11.3	vertical	yes(2)	yes	flood
4	15 May	1722	2.7	vertical	no	yes	flood
5	16 May	1017	2.7	horizontal	no	no	ebb
6	16 May	1050	2.7	horizontal	yes(1)	yes	ebb
7	16 May	1244	8.5	horizontal	yes(1)	yes	ebb
8a	16 May	1410	13.1	horizontal	no	yes	slack

Figure 5 illustrates the array configuration for the first four runs, conducted on 15 May, where the placement of the thermistors was vertical. Figure 6 illustrates the configuration of the array on the second day, 16 May, when the thermistors were in a horizontal line. Run 6 was conducted in this configuration but in all subsequent runs the array was rearranged such that Thermistor 1 was removed and placed 24 inches (60.8 cm) below Thermistor 5.

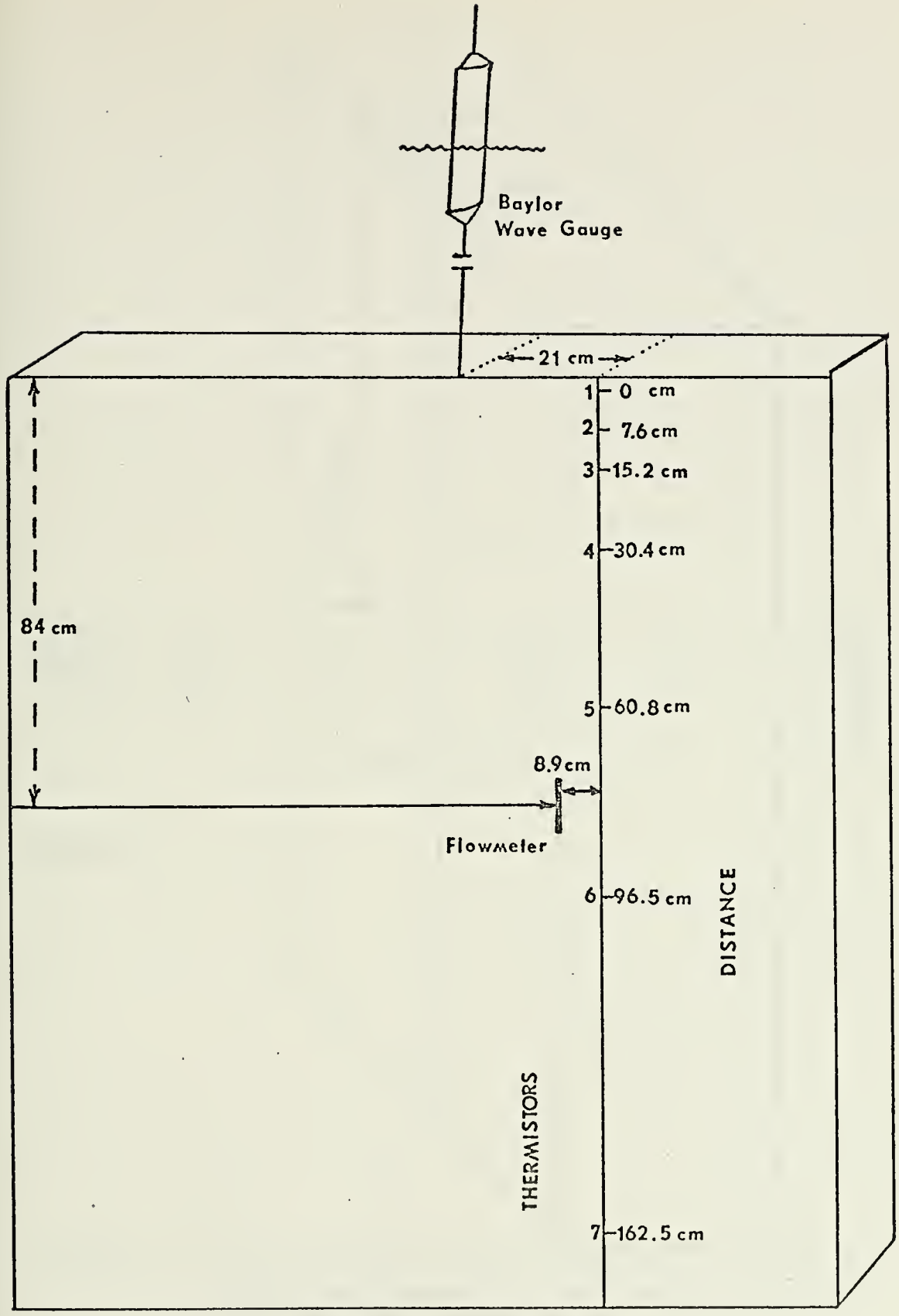

Figure 5. Configuration of Array for Runs 1, 2, 3, 4.

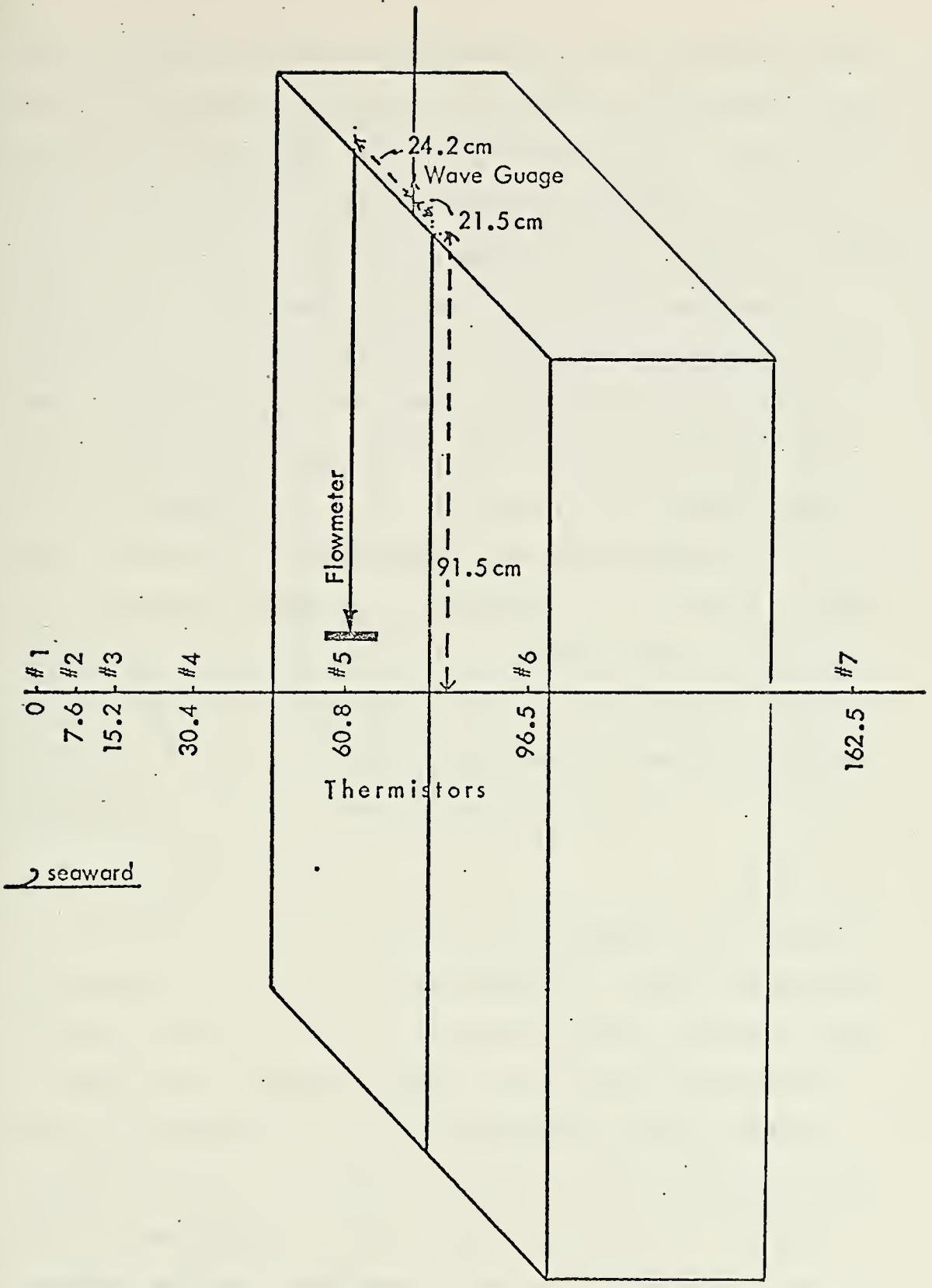

Figure 6. Configuration of Array for Run 6. For Runs 7 and 8a, Thermistor 1 was removed and placed 60.8 cm below Thermistor 5.

This was done to give an indication of the vertical temperature gradient. Data were recorded on a Sangamo 3562 analog tape recorder using F.M. electronics. These data were played back at 60 ips (32 times speed-up) and digitized at NPS on a hybrid (analog-digital) computer, CI5000 /XDS 9300. The sampling rate of the data analyzed was reduced to 6.25 Hz leading to a Nyquist frequency of 3.1 Hz. This reduction was not considered critical, since the spectra became essentially flat and the signal lost in noise before the 3.1 Hz frequency was reached. Data were analyzed on the school's IBM 360-67 computer. The environmental conditions consisted of light winds, small amplitude waves and swell, low overcast skies, and occasional internal waves during the two day period. Further details of both the experimental set-up and the analysis particulars can be found in Minard (1973).

B. DATA PREPARATION

Initially all the signals were graphically displayed on an eight channel strip recorder for visual inspection of the records, polarity, error and anomaly checks. Confirmation was made that runs 5 and 8 were unusable for digital purposes. Run 9 was designated Run 8a and replaced Run 8, for analysis purposes, since they were made at the same depth with the same configuration and in nearly the same time frame. The analysis was carried out using the nine-track digital tapes previously prepared from the analog records by Minard (1973).

C. METHOD OF ANALYSIS

The variances and covariances were calculated from the time series of each run by first removing any long period trend and any D.C. bias component. In addition, some of the time series were digitally high-pass filtered to filter out waves of period greater than 100 seconds prior to computation. Spatial correlations were computed by averaging the covariance (C.V.) between the first thermistor and each of the others such that:

$$C.V. = \frac{1}{T} \int Th_1(t,x) Th_i(t,x+\Delta x_i) dt$$

where T is the length of record ($\doteq$ 20 min). The C.V. was then plotted against the appropriate separation distance along the array using the first thermistor as a reference. The variances and covariances were normalized with respect to the variance of the first thermistor in the array. Both the normalized and the unnormalized spatial correlation functions were Fourier transformed to obtain the normalized and unnormalized wavenumber spectra for the runs.

Next, the gradients present in Runs 1, 4, 7, and 8a were calculated since they were to be used in the theoretical wave-induced temperature spectrum calculation. First, the digitized signals had to be re-converted to a true temperature since during the recording and digitizing processes a number of gains and biases had been

introduced. The original temperature recording had been a voltage conversion of the temperature variation around a balance resistance in the wheatstone bridge circuit of each thermistor. Therefore, the actual temperature would have been of the form

$$T = \bar{T} + \Delta T \ ,$$

where the overbar indicates the mean temperature and ΔT is the variation about the mean.

In San Diego, all signals were amplified before recording. Therefore the recorded signal would be $G1 \cdot \Delta T$, where G1 was the appropriate gain. During the digitizing process a bias (B1) was applied prior to the computer gain (G2), which was wired into the analog circuitry. The digitized signal, in terms of the original fluctuation, would be

$$D.S. = G2(G1 * \Delta T + B1) \ .$$

The original temperature in terms of subsequent biases and gains would be

$$T = \bar{T} + \left(\frac{D.S. - B1*G2}{G2*G1} \right) \ .$$

The gradients were then calculated for the selected runs using the temperature difference between thermistors 1 and 5, which had a constant spatial separation of 24 inches (0.6 m), as representative of the whole array.

A separate program was written to perform the spectral analysis of the time series. The data were read into files corresponding to Thermistor 5 and the Baylor Wave Gauge. The records were then detrended and the mean removed. Autocorrelation functions for each file and a crosscorrelation function between them were calculated. The autocorrelations were normalized with respect to their variance and the crosscorrelations with respect to the square-root of the product of the individual file's variances. From these functions, the auto- and cross-spectra were calculated by Fourier transforming the respective temporal correlation functions, after application of a Parzen window filter to account for the finite length of the time-series.

From the Baylor Wave Gauge spectrum, the wave-induced temperature spectrum was calculated using the spectral transfer function derived in Equation (5). In addition, coherence and phase angle were calculated between the temperature and waves. The theoretical turbulence spectrum was calculated from the difference between the actual temperature spectrum and the wave-induced temperature spectrum as given in Equation (9).

IV. RESULTS

A. ANALOG TEMPERATURE RECORDS

Examination of the analog records of temperature, reproduced in Figures 7 (Run 6) and 8 (Run 1), show that an internal wave was present in Figure 7 and not in Figure 8. The common features of each are the high levels of temperature fluctuation and the general consistency of prominent features throughout the temperature array.

B. TEMPERATURE FIELDS

Some long term fluctuations were noticed on all runs and four runs (2,3,6,7) show significant internal wave activity.

Runs 1 and 4 show patches of increased turbulence which may or may not have been remnants of internal waves. In any case, the scale of the turbulence was such that the whole of the vertical array was affected. Figure 9 is a plot using the digitized data of the first 15 minutes of Run 1 with a data point plotted every 4 seconds. The total vertical extent of the array covered 1.625 meters and over such a short distance the temperature difference between thermistors was never greater than 0.5°C and usually less.

Figure 10, a plot of the isotherms for Run 1, was made by converting each thermistor signal to an actual

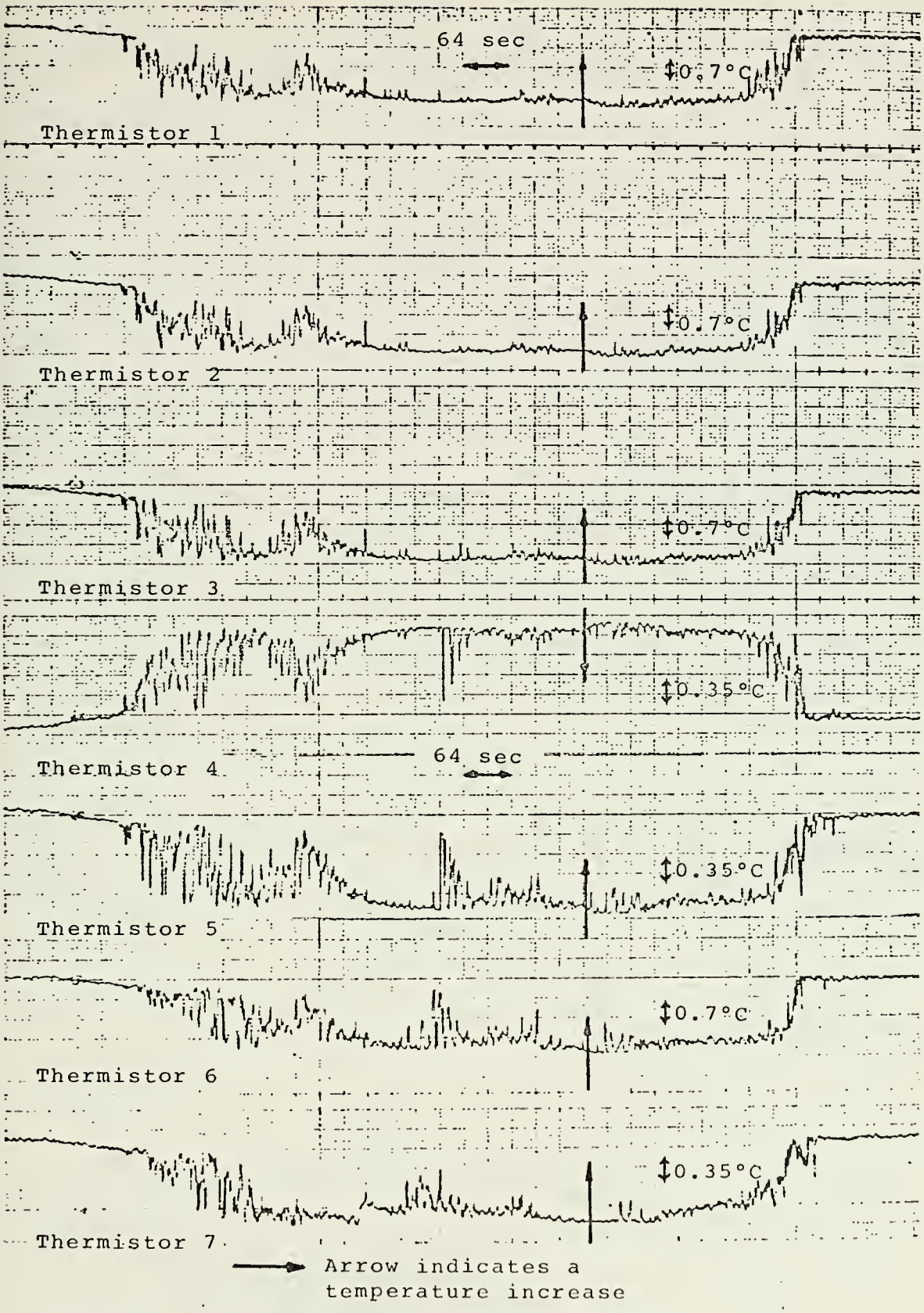

Figure 7. Analog Temperature Record-Run 6.

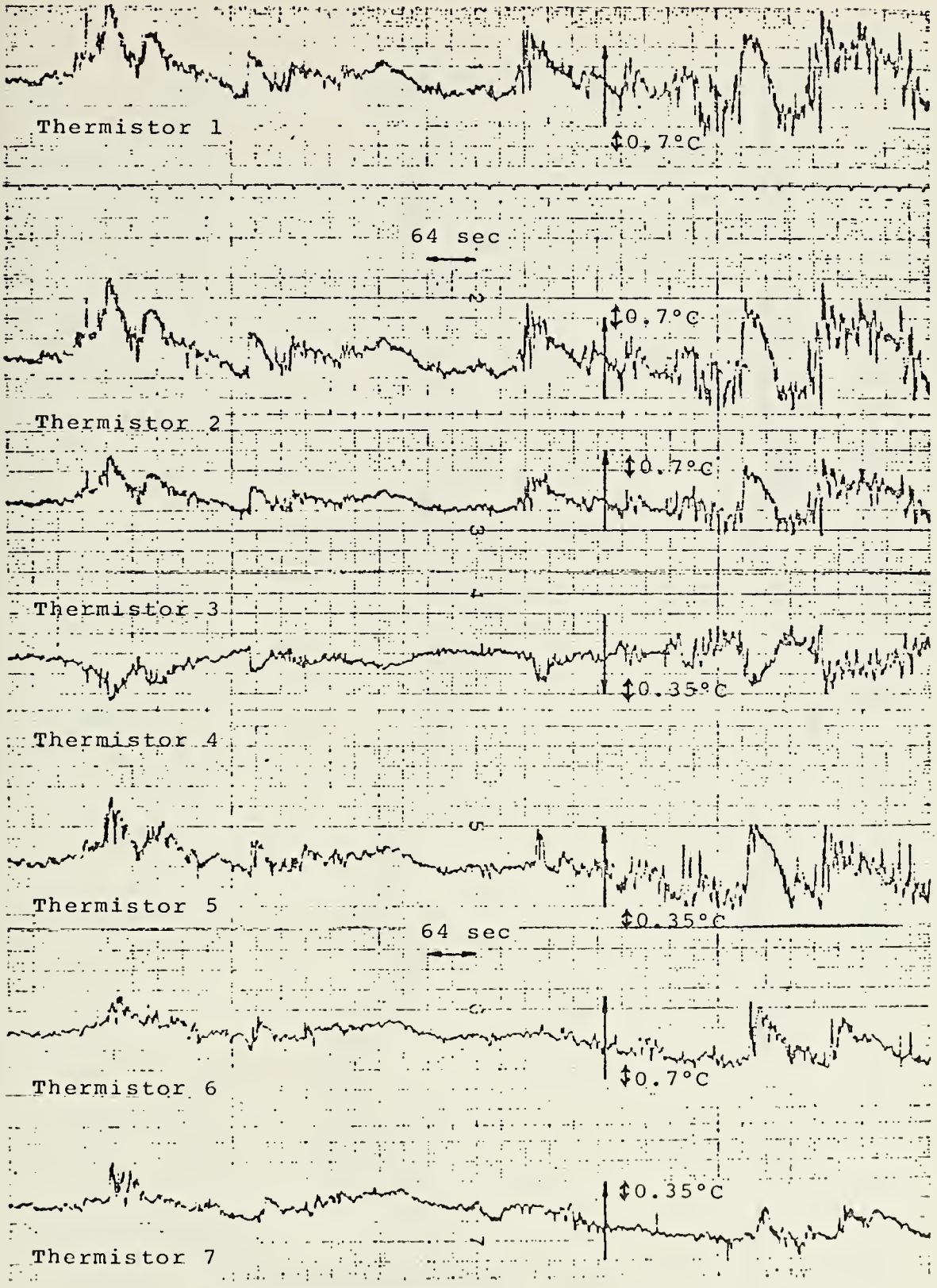

Figure 8. Analog Temperature Record-Run 1.

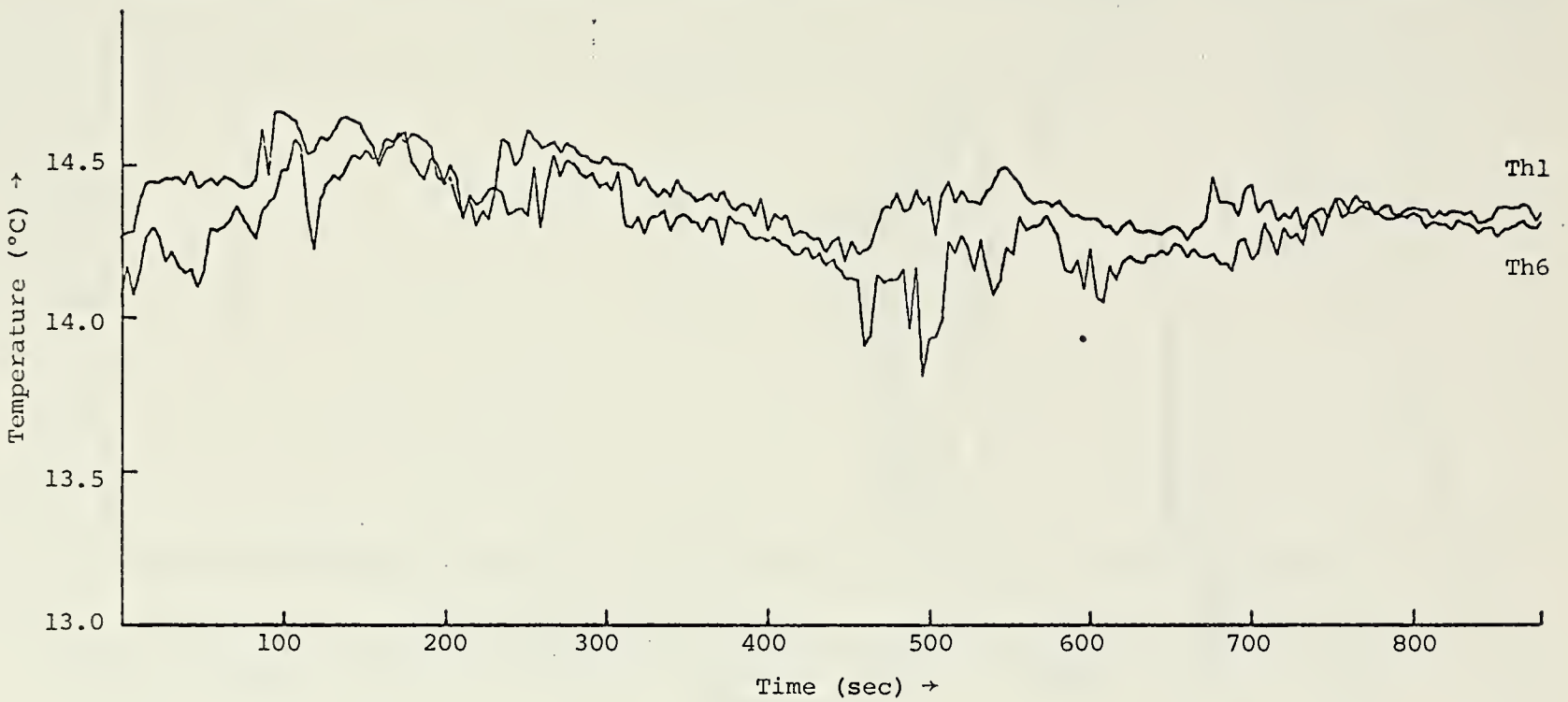

Figure 9. Digital Temperature Record, Run 1, Thermistors 1 and 6.

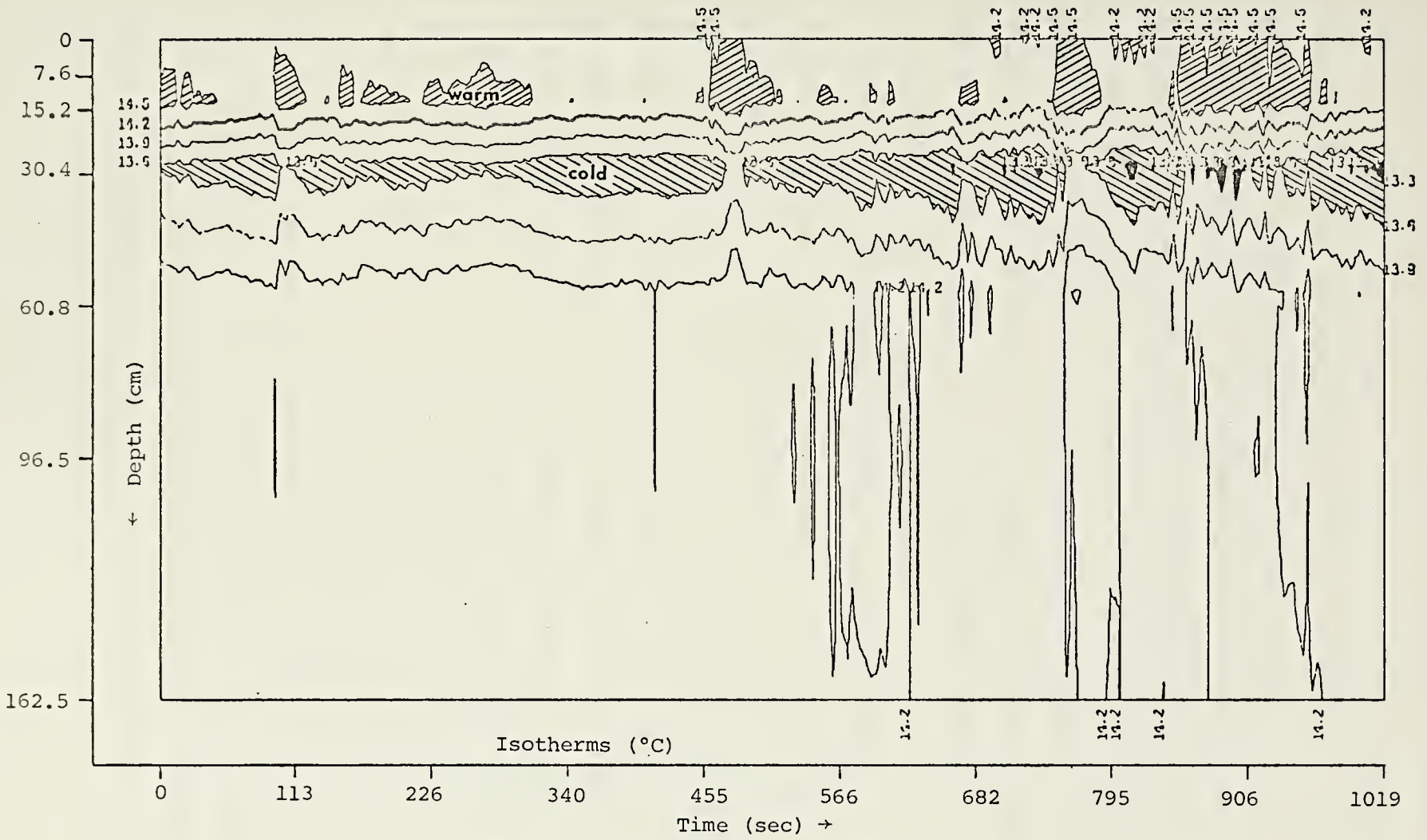

Figure 10. Isotherm Contours, Run 1.

temperature reading in the manner described in Section III-B. Subroutine "CONTUR", from the School's IBM/360 source library, was used to plot the isotherms at intervals of 0.3°C with a data point every 4 seconds of real time. The temperature data from the time series was linearly interpolated every 3 inches across the array, at each time increment, as input to the subroutine. The plot shows a relatively warm layer for the first 15 cm, underlain by a relatively cold layer in the next 15 cm, which in turn is underlain by a relatively warm layer covering the rest of the array.

Although no measurements were made of salinity in the detail required to solve this question, the salinity gradient must be slightly positive or at least isohaline for the first 30 cm of the array, and then increasingly positive to at least 60 cm in order for this system to be dynamically stable. If this is the case, then the possibility of double-diffusion type microstructure, with stable stratification and convective mixing within each layer, exists between the central and lower layer. The increased gradient of temperature between 15 and 30 cm is consistent with an inherently stable double-diffusion mechanism. If, in fact, the salinity gradient is negative in the first 30 cm then the possibility of salt-fingering exists (inherently unstable double-diffusion), although there is no direct evidence in the isotherm field to suggest this mechanism is occurring.

The decrease in the temperature gradient in the lower half of the array (Figure 11) may be an artifact produced by the array spacing and the subsequent interpolation of points in the contour plot.

The blobular formations within the warm upper layer and in the cold central layer are probably due to interactions with small amplitude internal waves which were not recognized as such from the temperature records alone. It would appear that the layers are being alternately squeezed and relaxed with a periodicity approximating 3 minutes. These blobs compare well in time to the increases and decreases in the turbulent temperature evident in Figure 9.

Runs which show significant internal wave activity are itemized in Table II by run number and "periodicity" measured from the analog records. Periodicity is at best

TABLE II. Internal Wave-Periodicity

run number	period (sec)
2	1350
3	1050
6	1450
7	1300

approximate due to the limited number of internal waves per record. Figure 11 is a plot of the first 15 minutes of Run 3 showing the temperature variation for Thermistor 1

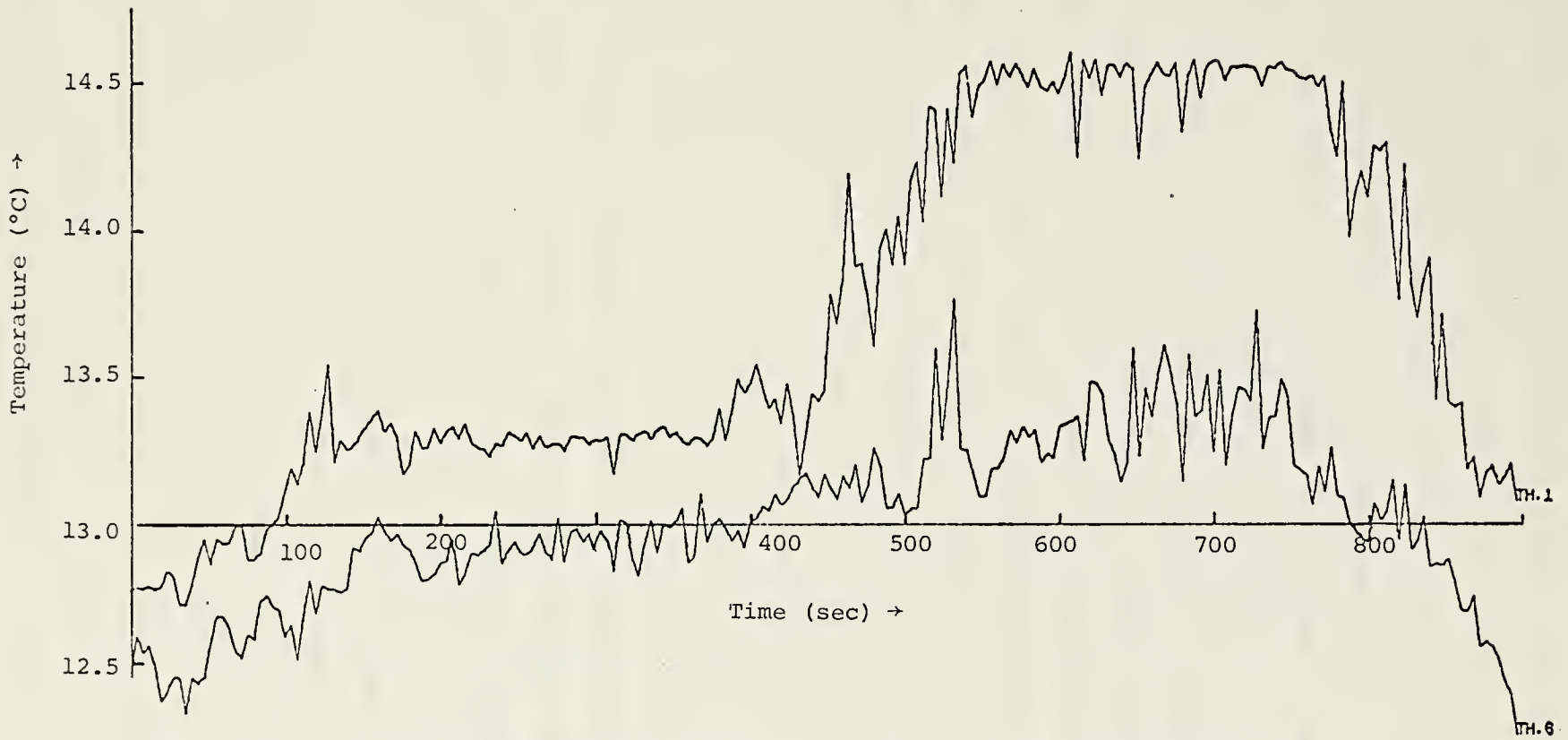

Figure 11. Digital Temperature Record, Run 3, Thermistors 1 and 6.

(top of the array, at 11.3 meters below the surface) and Thermistor 6 (towards the bottom of the array). One internal wave had just finished at the start of the plot. A second was starting at the end of the plot and continues into Figure 12, the next 15 minutes of Run 3. It illustrates the periodicity of the internal wave. Figure 13 is the computer plot of the isotherms for the first 15 minutes of Run 3. The intrusion of colder water into the upper portions of the array and its subsequent withdrawal as the internal wave passes is quite noticeable. The salinity profile corresponding is unavailable but is probably a positive or isohaline gradient with increasing depth. Double-diffusion type microstructure would not be present under these conditions of stratification and billow turbulence microstructure would be more likely.

The thermistor array during Run 3 was located just below a slight thermocline which had been decreasing in depth and, to some extent, intensity from the time of Run 1(Minard 1973-Figure 1). This suggests that the presence of internal waves in the period of time from Run 1 to Run 3 was contributing to the depression and erosion of the thermocline. Figure 13 shows the extreme variability and fluctuation in an individual isotherm. Some of the fluctuation is no doubt attributable to turbulence which could be a cause of the thermocline erosion. However, the assumption that the fluctuations are solely caused by turbulence must be tempered to some degree

Figure 12. Digital Temperature Record, Run 3, Thermistors 1 and 6.

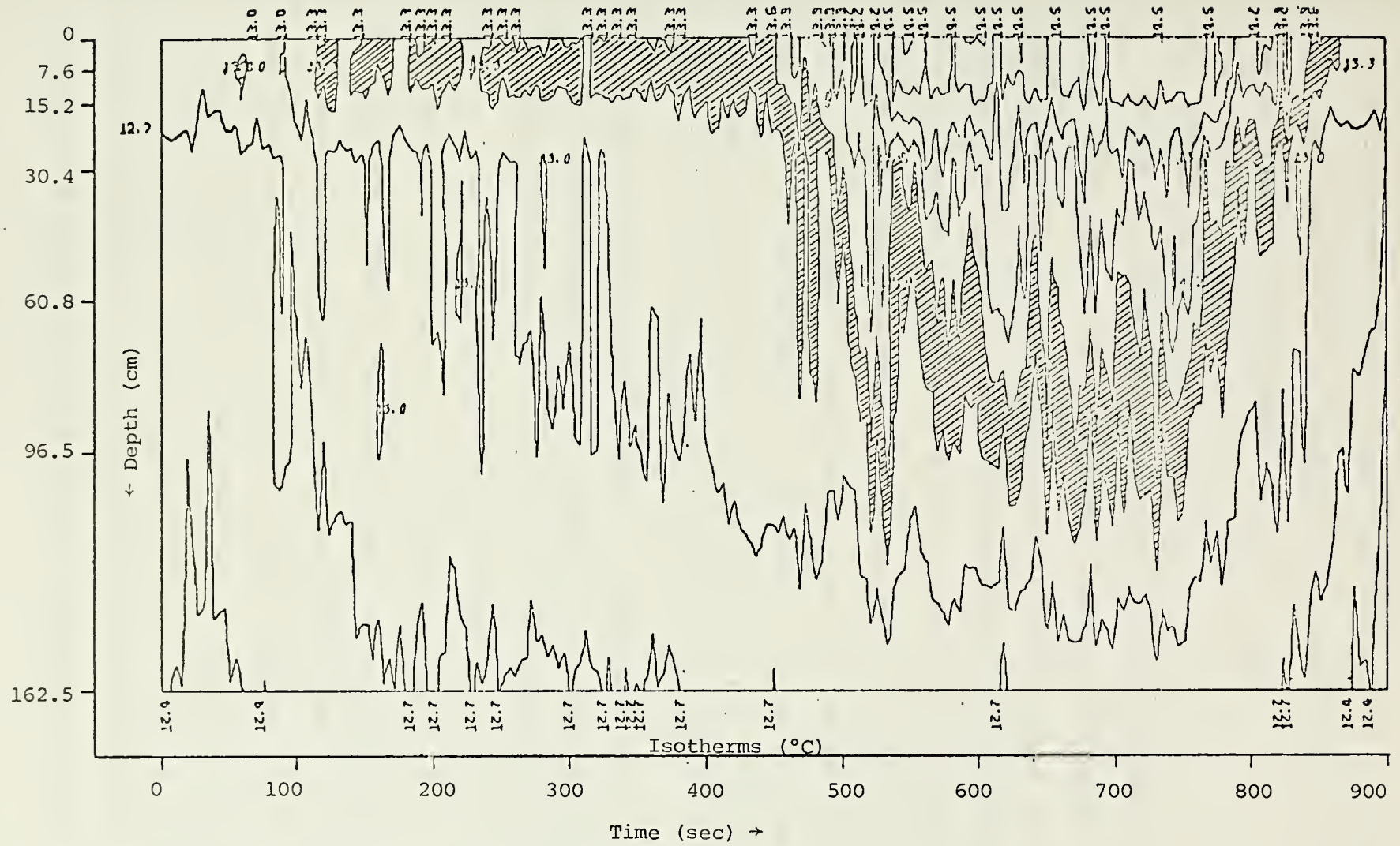

Figure 13. Isotherm Contours, Run 3.

since successive peaks in the fluctuations are separated by about 12 seconds, a figure that is suspiciously close to the surface wave period.

C. SPATIAL CORRELATIONS

Table III contains a listing of the covariances between Thermistor 1 and the others, and the individual variances of each thermistor, for all of the runs for both non-filtered and high-pass filtered data. To accomplish the high-pass filtering, a Fourier analysis was made of each 20 minute segment of data; the Fourier coefficients generated were used to generate a time series describing the waves of 100 seconds and greater. This series was then subtracted from the original time series which was then the filtered time series used for analysis.

One of the most common ways to define a scale length of some inhomogeneity is to measure the length required for the correlation to fall to 1/e (0.368) of its original value. The correlation functions, shown in Figures 14 and 15, are of a very long scale feature and only one run in each figure actually falls to 0.368. This phenomena is interpreted as being due to the extremely long scale of the internal waves and their attendant higher overall energy. Consequently it was decided to filter out the waves of periods 100 seconds and longer. This was accomplished digitally, as explained earlier. The results, after the digital filtering of the temperature signal,

TABLE III. Variance and Covariance

Thermistor	Lag Distance (cm)	Non-Filtered Covariance ($°C^2 \times 10^5$)	Non-Filtered Variance ($°C^2 \times 10^5$)	High-pass Filtered Covariance ($°C^2 \times 10^5$)	High-pass Filtered Variance ($°C^2 \times 10^5$)
Run 1 - Depth 2.7 m					
1	0	927.85	927.85	913.9	913.9
2	2	896.64	930.09		
3	6	873.64	950.88	377.8	204.8
4	12	888.45	1037.10		
5	24	835.04	1143.21		
6	38	778.95	1514.08		
7	64	567.37	1866.73		
Run 2 - Depth 5.2 m					
1	0	1896.44	1896.44	334.7	334.7
2	3	1938.24	2015.72		
3	6	1946.45	2075.39	147.1	89.4
4	12	2021.25	2260.11		
5	24	2092.34	2492.25		
6	38	2150.95	2717.21		
7	64	1268.59	1054.74		
Run 3 - Depth 11.3 m					
1	0	41043.4	41043.4	532.9	532.9
2	3	40930.5	41515.1		
3	6	39599.6	39250.9	372.1	644.9
4	12	35313.0	32636.5		
5	24	28213.9	22285.1		
6	38	22516.4	15548.2		
7	64	11846.2	4352.2		

TABLE III (continued)

Run 4 - Depth 2.7 m					
1	0	402.14	402.14	64.54	64.54
2	3	396.90	415.90		
3	6	237.69	158.99	34.44	24.61
4	12	396.10	465.16		
5	24	225.14	191.22		
6	38	232.62	292.28		
7	64	184.52	234.96		
Run 6 - Depth 2.7 m					
1	0	65222.2	65222.2	6392.0	6392.0
2	3	66039.8	67783.1	5504.7	6304.9
3	6	62945.9	62468.0	4787.2	6434.9
4	12	63141.2	64784.7	2711.5	3399.3
5	24	58157.1	57796.2	1667.7	5155.3
6	38	56955.3	57332.0	1475.8	13112.5
7	64	35995.8	22536.5	271.8	5232.9
Run 7 - Depth 8.5 m					
2	0	* 8552.9	*10716.6	4394.5	4394.5
3	3	*85312.2	*10351.7	3829.0	4102.3
4	9	* 7506.0	*29226.8	2046.3	1852.0
1	21	*10666.7	*10666.7		
5	21	* 8311.3	*15462.8	1567.6	1903.6
6	35	* 6813.9	*26134.1	1655.4	2229.4
7	61	* 4699.0	* 9192.8	1399.7	1910.9
Run 8a - Depth 13.1 m					
2	0	* 156.27	* 198.9	117.1	117.1
3	3	* 93.60	* 108.3	83.5	87.9
4	9	* 47.0	* 159.9	41.29	34.2
1	21	* 229.75	* 229.75		
5	21	* 116.1	* 145.8	25.11	28.7
6	35	* 50.0	* 208.9		
7	61	* 43.0	* 376.6	12.56	111.3

*Calculated WRT TH1 - not in "0" position.

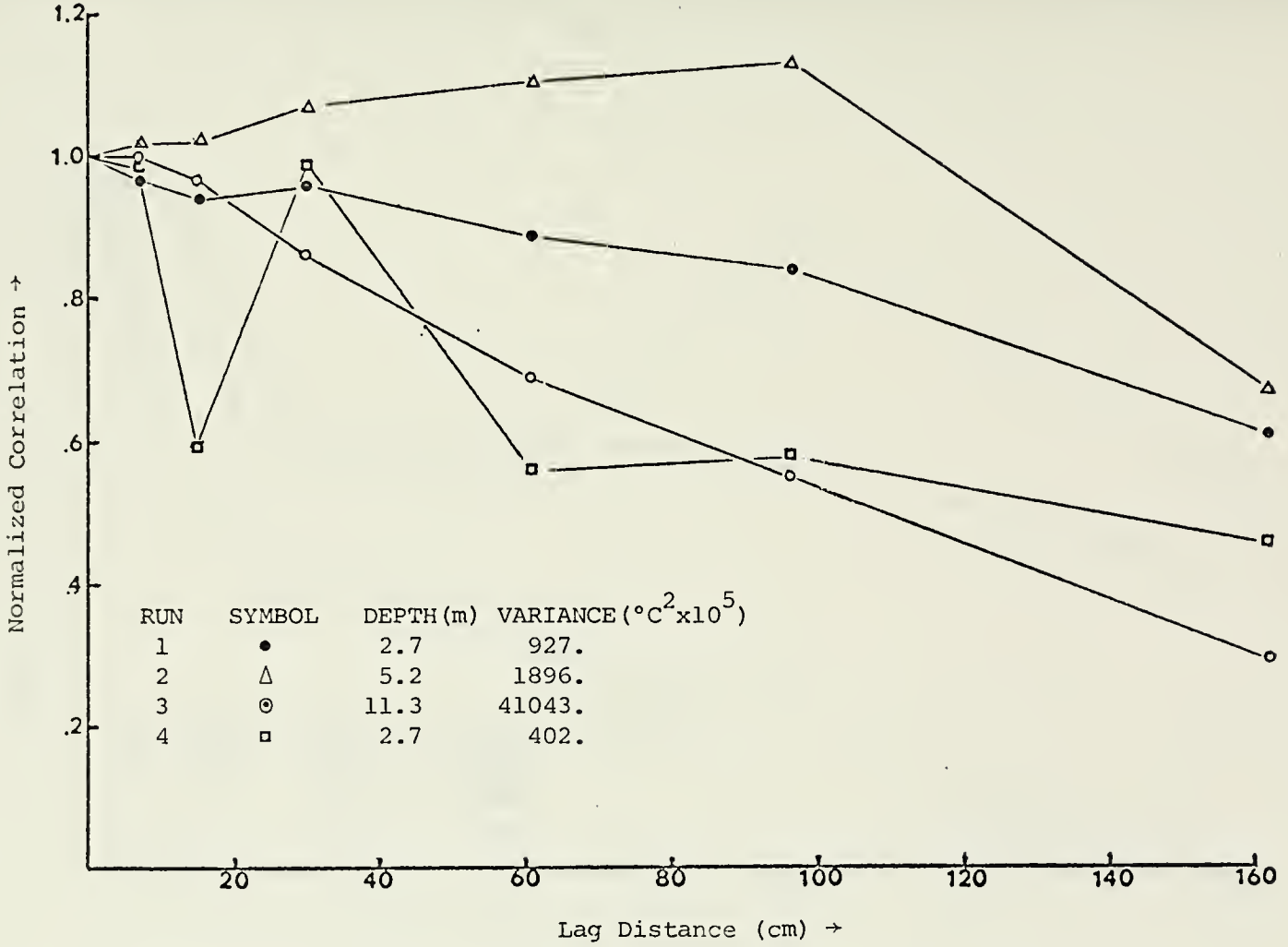

Figure 14. Non-Filtered Spatial Correlation-Vertical Array.

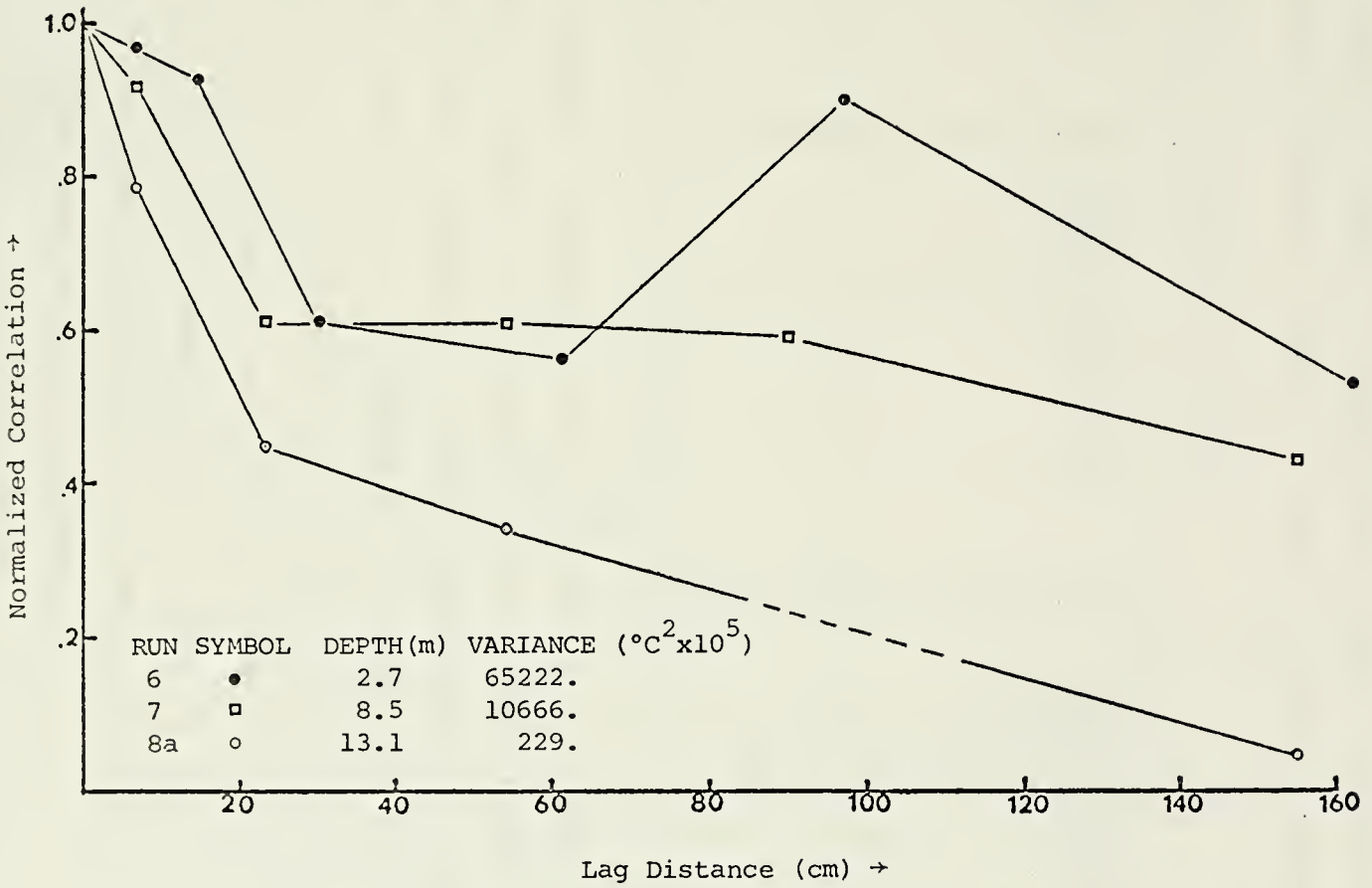

Figure 15. Non-Filtered Spatial Correlation - Horizontal Array.

are illustrated in Figures 16 and 17 where it is apparent that waves of 100 sec and longer had been contributing substantial energy as evidenced by the overall lowering of the spatial correlation curves when filtered.

Table IV lists the correlation lengths for each run after the original signal had been high-pass filtered.

TABLE IV. Correlation Lengths

Run Number	Depth-Surface to Top of Array (m)	Correlation Length (cm)
1	2.7	100.5
2	5.2	100.5
3	11.3	35.2
4	2.7	130.5
6	2.7	40.0
7	8.5	50.0
8a	13.1	21.4

Although it might be expected that the shortest correlation lengths would occur at the surface, where waves dominate the structure, no such relationship is apparent. Perhaps this can be explained by the fact that the array dimensions are small compared to the depth and breadth of the surrounding ocean area; or the scale of the turbulence may be quite large compared to the depth of the water; or maybe it further illustrates that waves do little mixing but only pump the water up and down.

A consistent trend was noticed in that the horizontal array always had shorter correlation lengths than the

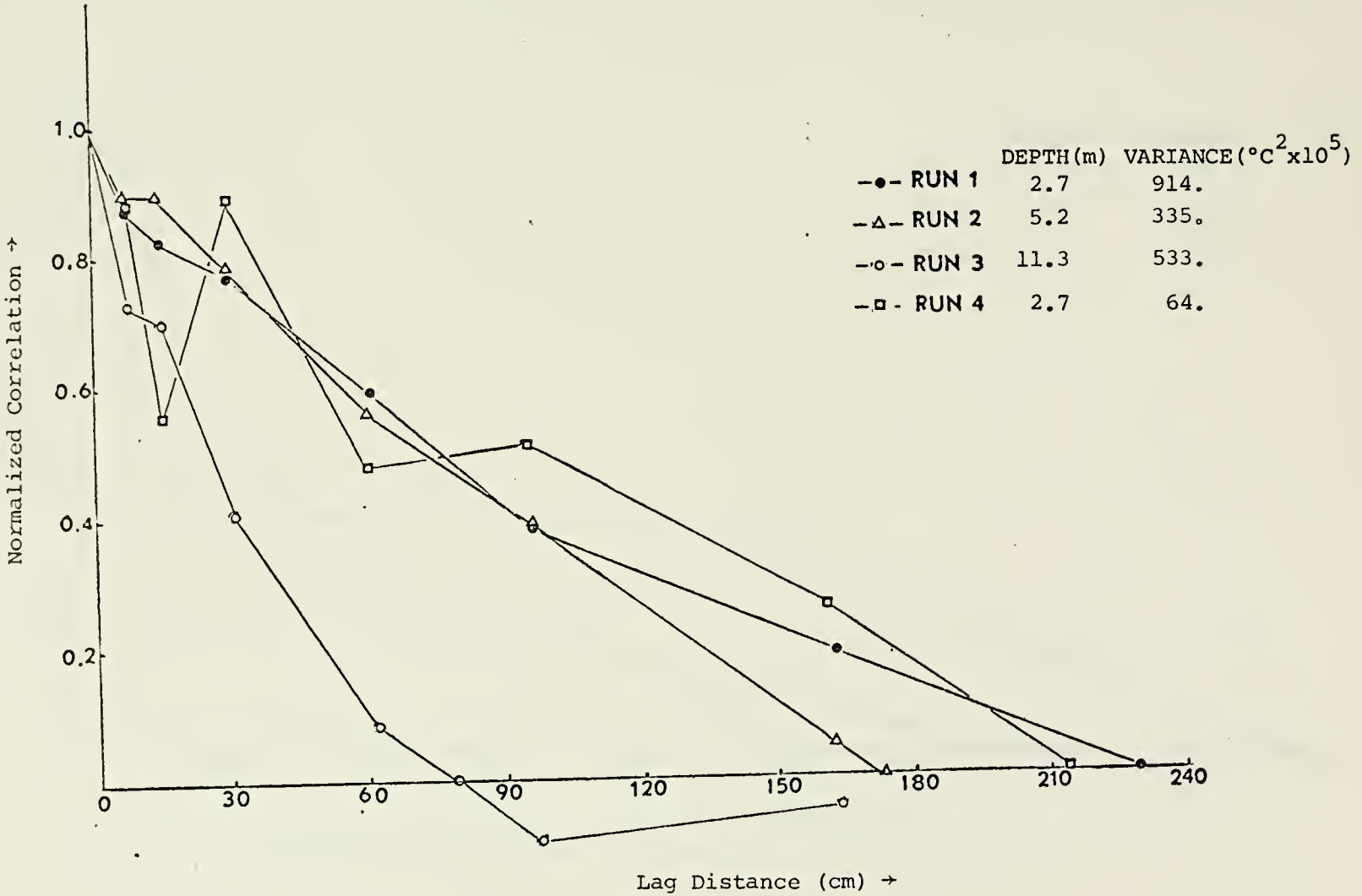

Figure 16. Spatial Correlation (Vertical Array).

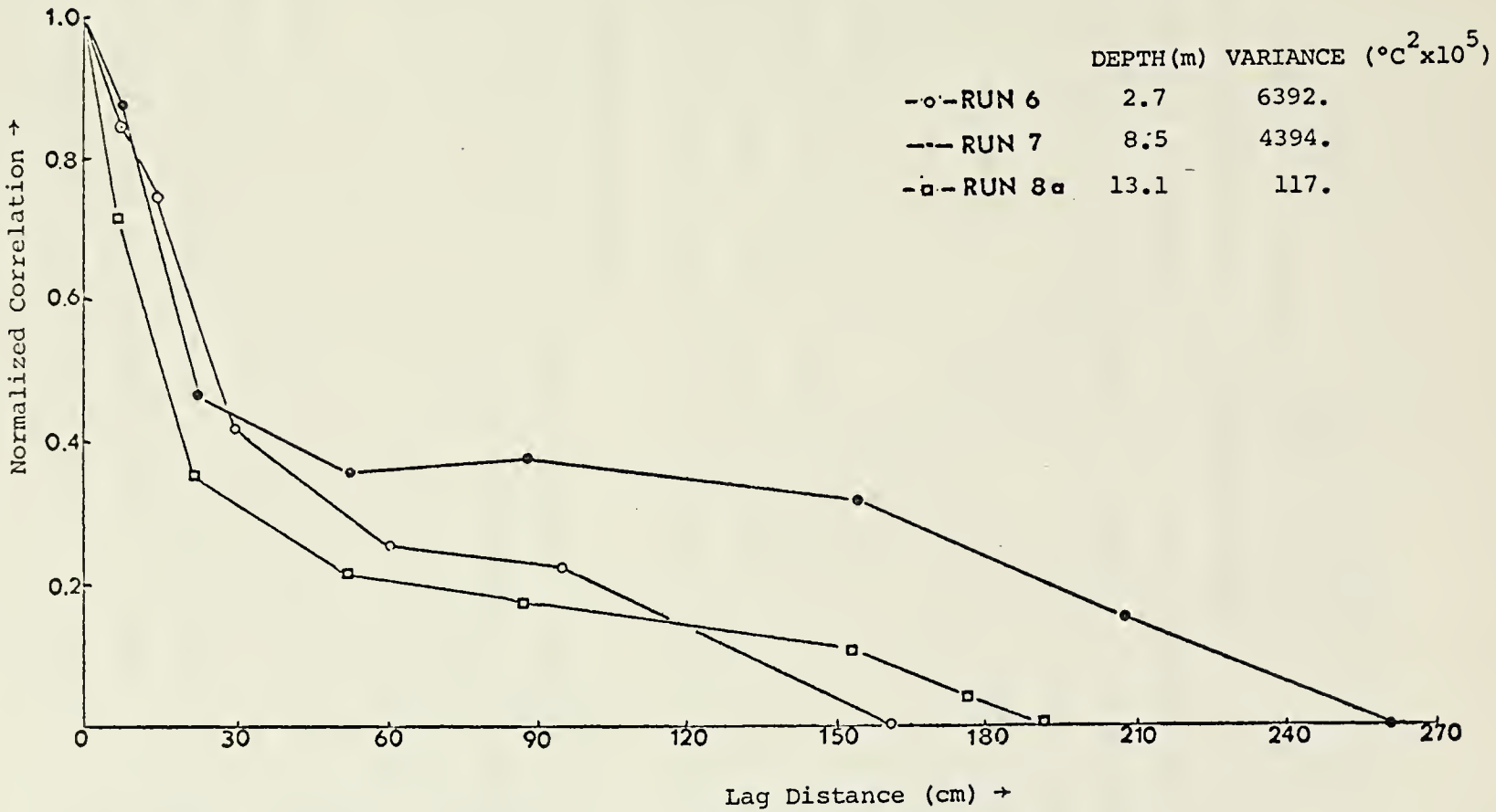

Figure 17. Spatial Correlation (Horizontal Array).

vertical array at similar depths. However, this result is not conclusive since horizontal and vertical array runs were made on different days.

Further examination of Table III shows that the runs with significant internal wave activity have higher energy as evidenced by the higher numerical values of variance and covariance. This trend is present even when the signal was filtered for waves of 100 sec and greater except that Runs 2 and 3 are not significantly greater in energy than Runs 1, 4, and 8a. This indicates that Runs 6 and 7 contain significantly more energy at all frequencies than Runs 2 and 3. Also the difference in covariances between signals not filtered and filtered show that Runs 1 and 8a contained much less energy at periods greater than 100 sec than any of the other runs.

D. WAVENUMBER SPECTRA

The normalized wavenumber spectra were calculated by Fourier transforming the spatial correlation functions (Figures 16 and 17) calculated as explained in Section III.B. The spatial correlation was calculated at equal increments along the length of the array by linearly interpolating between the calculated points on the array. Figure 18 is a composite of the normalized wavenumber spectra when the array was vertical (15 May); and Figure 19 is a composite when the array was horizontal (16 May).

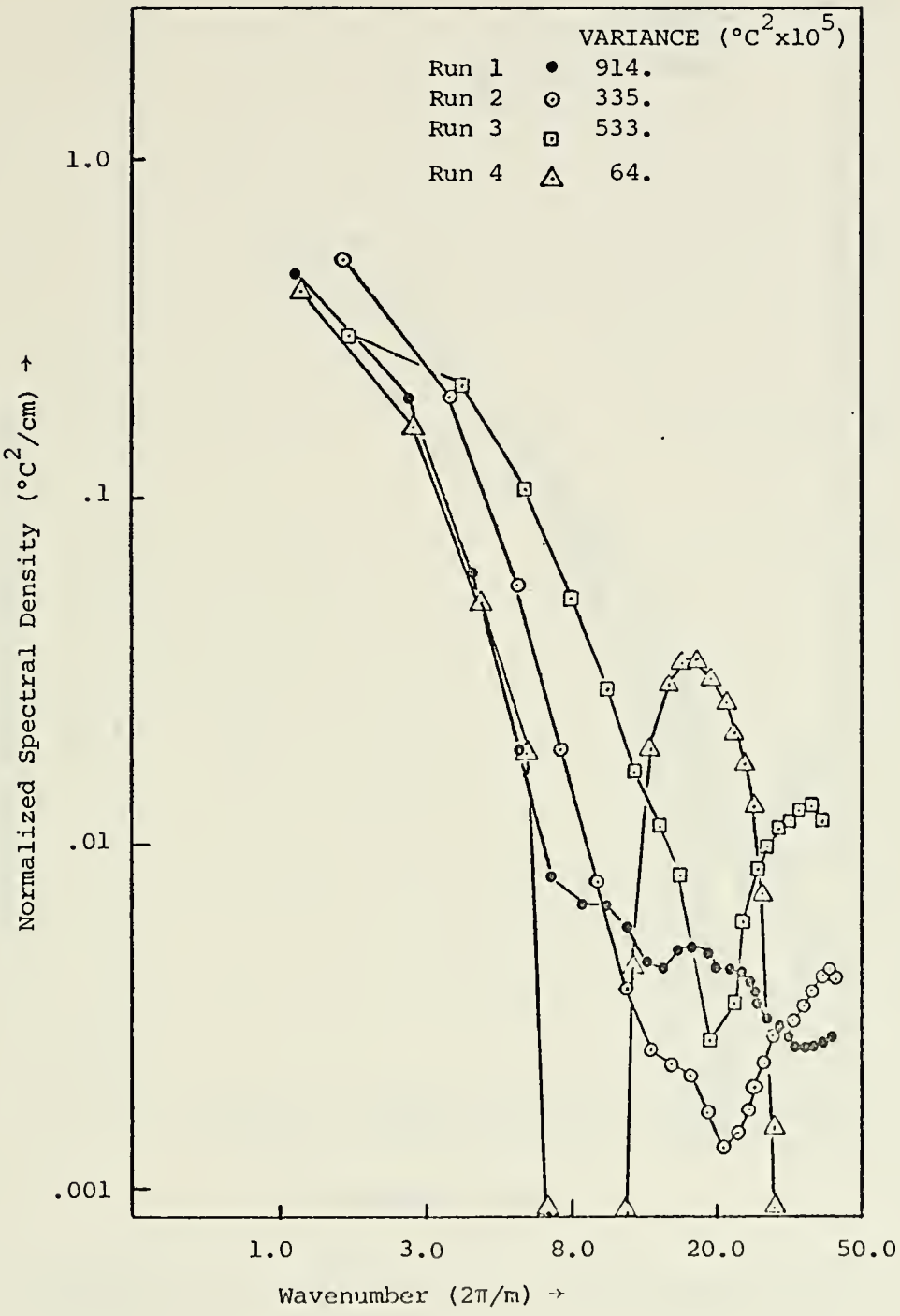

Figure 18. Vertical Array Wavenumber Spectra.

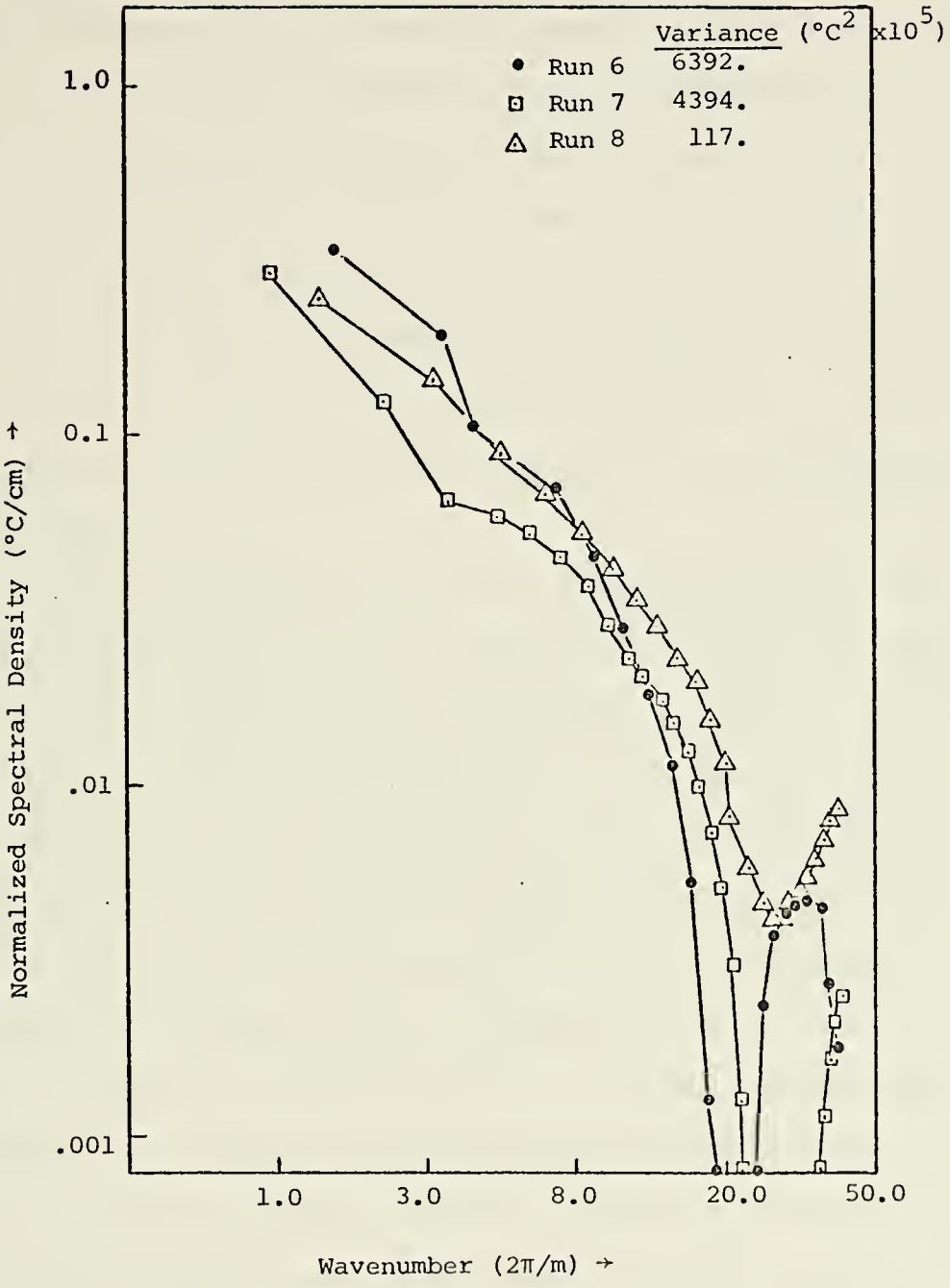

Figure 19. Horizontal Array Wavenumber Spectra.

The spectra show a high degree of consistency between runs. In the vertical array, Runs 2 and 3 show slightly more energy at all wavenumbers than Run 4 but less energy than Run 1. It would appear that Run 4 had a major portion of its energy at periods greater than 100 sec as was the case for Runs 2 and 3 with the internal waves. In the horizontal array spectra, all runs are very similar in shape whereas the vertical array spectra varied considerably in shape. It is felt that this may be interpreted as a difference in the source of turbulence on the two days.

Each of the spectra has what is believed to be an anomalous spectral energy increase at higher wavenumbers. Gregg, Cox and Hacker (1973) observed a similar increase at slightly higher wavenumbers in the temperature gradient spectra. They attributed the initial rapid fall-off, below 0.06 radians per meter (rpm), to dynamical processes dominated by the nearly exponential mean temperature gradient with depth. For wavenumbers greater than 0.06 but less than 31.4 rpm they felt the spectrum was dominated by the irregularly spaced high gradient regions. In the region of interest, above 31.4 rpm, where high levels of microstructure exist the spectrum takes the form of a minimum followed by a maximum at higher wavenumbers. This last region is in general the same wavenumber space as the increase in our spectrum. Whether the increase is due to

the same cause is uncertain; but there were high levels of microstructure activity in all the runs. However, it may be that this increase is due to other factors such as the manner in which the correlation function was calculated in deriving the spectrum. No attempt was made to fit the correlation function to other interpolation forms, e.g., Gaussian or exponential, near the origin since the structure function when calculated did not show that the time series were particularly stationary.

It seems reasonable that the wave-induced contribution to the wavenumber spectra would occur over a narrow frequency band corresponding to the frequencies of high coherence in the frequency spectra. Consequently, the spatial scale in wavenumber space should show correspondence to the orbital excursion of the wave-induced particle motion within this narrow band. The scale of the particle displacement is calculated using the root-mean-square (rms) wave height in each run. The vertical displacement, $\xi(t)$, using linear wave theory, is related to the wave profile, $\eta(t)$, by

$$\xi(t) = \left[\frac{\sinh k(z+d)}{\sinh kd}\right] \eta(t)$$

where the term in brackets is the spectral response function, $H_w(\sigma)$. The maximum displacement can be approximated at the peak in the frequency spectrum as

$$\xi_{max} = - \frac{H_w(\sigma)_{max} \eta_{rms}}{\partial\bar{\theta}/\partial z} , \qquad (12)$$

where $H_w(\sigma)_{max}$ is the response function at the frequency of maximum coherence and η_{rms} is the rms wave height. The horizontal excursions can be similarly calculated, using linear wave theory, as

$$\zeta(t) = [\xi_{max}] \coth k(z+d).$$

The results of these calculations are presented in Table V.

TABLE V. Particle Displacements

Run	Wave Height (m)	Depth of Th. 5 (m)	Freq. (Hz)	ξ_{max} (m)	Wave-number (rad/m)	ζ_{max} (m)	Wave-number (rad/m)	Expected wave-number (rad/m)
1	0.99	3.6	0.092	0.76	8.3	1.25	5.0	9.0
6	1.27	3.6	0.092	0.98	6.4	1.63	3.9	8.0
			0.214	0.66	9.5	0.66	9.5	8.0
7	1.52	9.3	0.092	0.68	9.2	1.63	3.9	6.0
8a	1.38	13.8	0.092	0.30	21.1	1.41	4.5	18.0

These scales are representative of the diameter of the water particle orbit. It would be expected that if there is a peak in the frequency spectrum (Figure 24) corresponding to surface wave-induced motion, then there should be a peak in the wavenumber spectrum associated with the same motion at the wavenumber of the excursion. Examination of Figures 18 and 19 shows that although there is no

peak in the spectra there is a definite change in the slope of each spectrum in the vicinity of the scale length calculated through Equation (12). The fact that the intersections do not lie exactly at the change of slope may be due to the use of the rms wave height rather than the median height or some other value. Also as would be expected, the scale length, ξ, decreases as the depth increases illustrating the decrease of the orbital motion with depth.

E. GRADIENT FIELDS

Gradients for Runs 1, 4, 7, 8a were calculated and the digital data plotted. Table VI is a compilation of the calculated mean gradient, the coherent gradient used in calculating the wave-induced spectrum, and the gradients as determined by Minard from the bathythermographs [Minard, 1973].

TABLE VI. Gradient Data

Run Number	Top of the thermocline (m)	Top of the frame (m)	B.T. gradient (°C/m)	Calculated gradient (°C/m)	Coherent gradient (°C/m)
1	4.25	2.7	0.98	0.93	.009
4	14.7	2.7	0.25	0.19	not calc.
6	0	2.7	0.44	not calc.	.096
7	14.5	8.5	0.11	-0.41	-.07
8a	5.0	13.1	0.54	0.10	.017

As can be seen from Table VI, the gradients taken from the Bathythermograph (BT) are in general agreement with the time-averaged mean gradient from the time-series, with the exception of Run 7. The difference can be accounted for because of the difference in length over which the gradients were determined. The gradient determined from the BT's was originally averaged over a distance of 18 meters and was all that was available, whereas the calculated mean gradient was determined over 24 inches (0.6 m), the distance between Thermistors 1 and 5 on all runs. The difference in length over which the gradient is calculated is important and can be illustrated from the results of Run 1. The mean calculated gradient was determined to be 0.93°C/m (Table VI). Figure 9 shows the temperature profiles of Thermistors 1 and 6 of Run 1 (same time frame but Thermistors 1 and 6 are separated by 14 inches (0.30 m) more than Thermistors 1 and 5). Here the maximum temperature difference is about 0.5°C, and since the separation was 38 inches (0.96 m) between thermistors, the gradient would be a maximum of 0.52°C/m. It can be seen from this that a small change in the length can result in a large change in the gradient.

It can also be seen that the BT and calculated gradients are much greater than the gradient required to match coherences in the wave-induced spectrum. This indicates that the spectral model would overestimate the wave-induced temperature fluctuations if the actual mean gradient were

used. Thornton et al (1974) noticed the same result and calculated the effect of buoyancy to try and account for some of the difference. They concluded that "buoyancy effects do not dampen the motion, but serve to amplify it relative to the homogeneous case." Hence they could not explain why the mean gradients are greater than the coherent gradients since the wave solution would be improved by less than 1% by including the buoyancy effects. What is obvious is that the specification of a constant mean gradient is not completely realistic in the presence of internal waves and turbulence.

Figure 20 is a plot of the digitized data of Thermistors 1 and 5 during the first 22 minutes of Run 1. Thermistor 1 was 0.6 m above Thermistor 5 and therefore a positive gradient is indicated, i.e., temperature decrease with depth. Figure 21 shows both the gradient and Thermistor number 1 temperature plotted together for the first 22 minutes of Run 1. Each point on the plot is the averaged gradient over 1.44 seconds. Thermistor 1 is replotted from Figure 20 but at a slightly different scale. The arrows labelled A and B in both Figures 20 and 21 serve to indicate noticeable points of gradient increase.

Figures 22 and 23 show the same information, as explained above, for Run 7 where Thermistor 5 is now 0.6 m above Thermistor 1. Again a point is marked (C) to illustrate an increase in gradient. What is interesting, however, is the difference in the temperature profiles and gradients between Runs 1 and 7.

Figure 20. Digital Temperature Record, Run 1 - Thermistors 1 and 5.

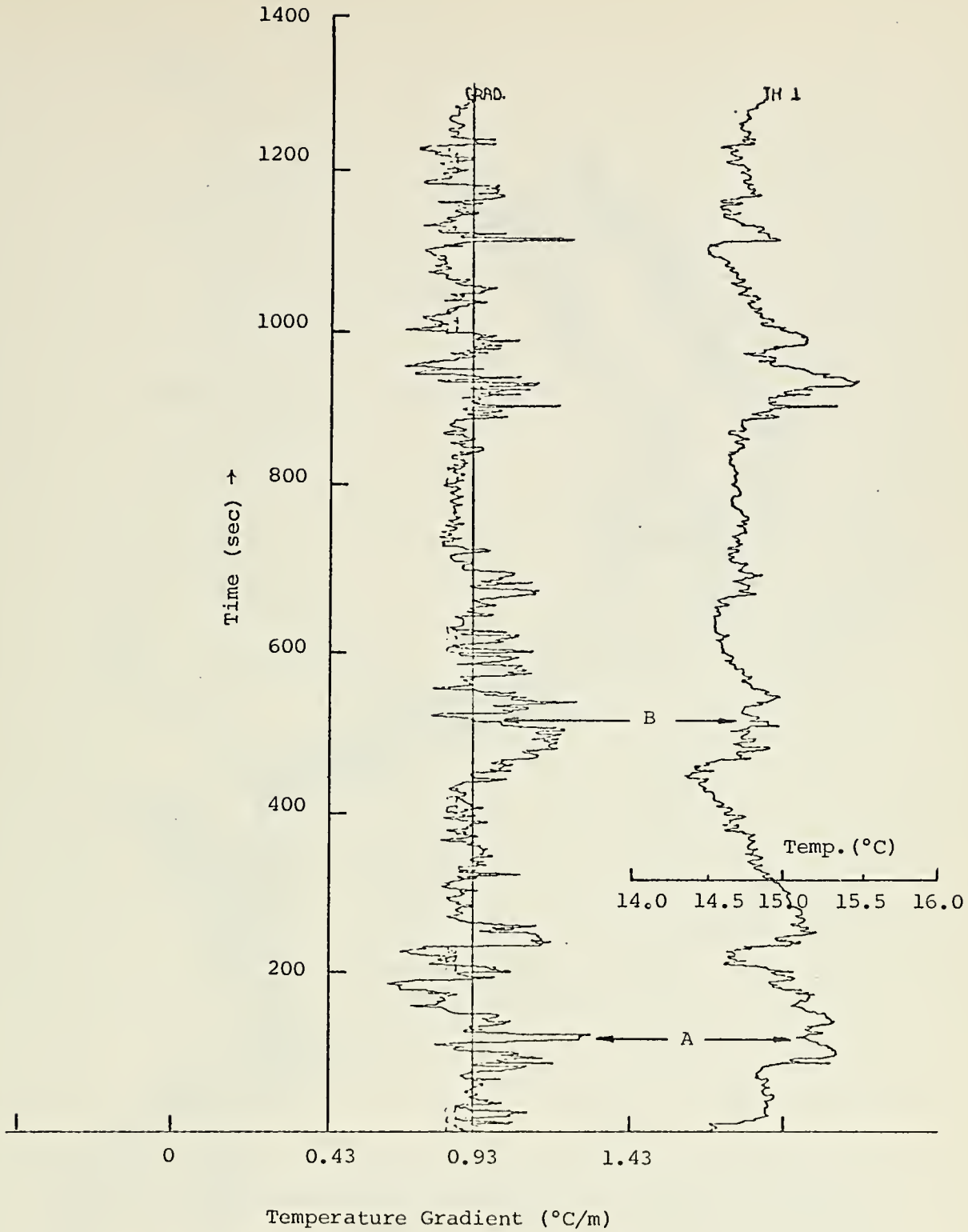

Figure 21. Temperature Gradient Plot, Run 1. Gradient between Thermistors 1 and 5, and Temperature Profile of Thermistor 1.

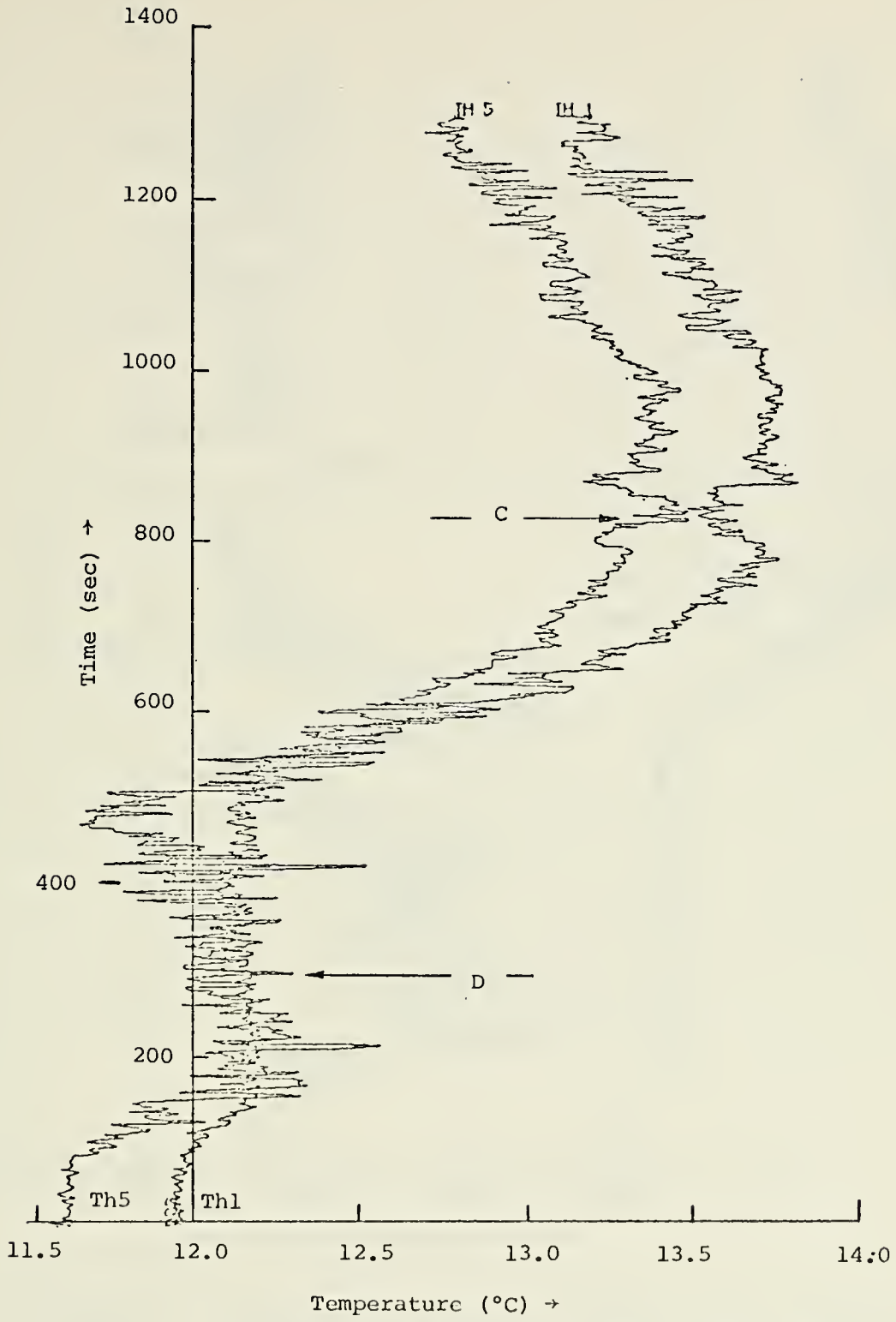

Figure 22. Digital Temperature Record, Run 7, Thermistors 1 and 5.

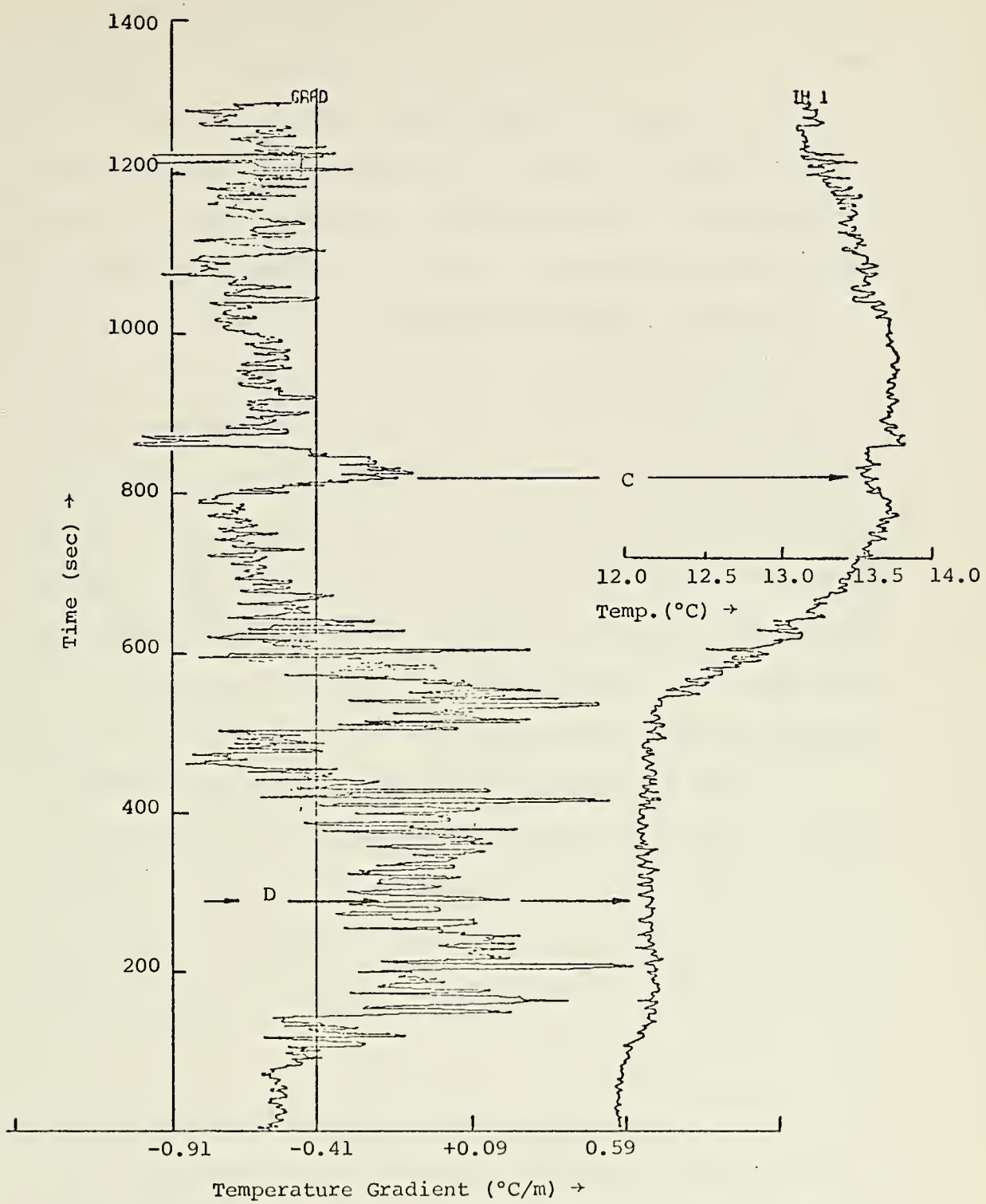

Figure 23. Temperature Gradient Plot, Run 7. Gradient between Thermistors 1 and 5 and Temperature Profile of Thermistor 1.

In Run 1, the temperature profile appears to be as 'turbulent' and perhaps more so than Run 7. Run 7, however, is marked at the beginning by the passage of an internal wave. The gradients in Run 1 are relatively constant, being uniformly positive with a deviation of less than 0.5°C/m from the mean. On the other hand, the gradients in Run 7 are extremely variable, being both positive (indicating stable conditions) and negative (indicating unstable conditions) with extremes ranging from +0.58 to -1.04°C/m. In addition, it appears that most of this record is best characterized as dynamically unstable. This is certainly indicative of intense turbulence associated with the internal wave and there may be some indication that the wave has 'broken'. In the area of point D on Figure 23, the gradient is almost zero for a period of nearly 150 sec and represents a zone of nearly homogeneous water brought about from the intense turbulent mixing. In an analog to surface waves, this zone could be termed an 'internal swash zone'. The calculated gradients for Runs 4 and 8a are similar to the results for Run 1.

F. TEMPERATURE FREQUENCY SPECTRA ANALYSIS

The results of Run 6 will be discussed more fully than the other runs since it most clearly demonstrates the effect of surface wave-induced fluctuations. The

other three runs analyzed (1, 7, 8a) will be discussed only insofar as they differ from Run 6.

1. Surface Wave-Induced Temperature Fluctuations

Equation (7) was used to calculate the wave-induced temperature spectra. Initially the mean temperature gradient, as calculated from the time-series, was used in the transfer function given in Equation (5). This led to an overestimation in the wave-induced temperature spectra. The variability in the temperature gradient field was considered to be mainly a function of the internal waves present and consequently the use of a mean gradient was hardly realistic. If an approximation to a mean gradient had to be used, it may have been better to use the median, or most commonly occurring, gradient. Since a statistical analysis of the gradient was not possible it was decided to use the method of establishing a coherent gradient as Thornton et al (1974) had done. Therefore, a gradient was used which matched the measured peak coherence value between waves and temperature with a calculated (theoretical) coherence using the calculated wave-induced temperature spectrum substituted into Equation (11). Their rational for doing this was that if the turbulent and wave-induced temperature fluctuations are statistically independent then the measured coherence should be closely approximated by this equation provided the transfer function was correct.

Since the model is based on linear theory the only "free variable" in the transfer function is the gradient. This coherent gradient (Table VI) is significantly different from the mean gradient. Table VII shows the appropriate values of depth, frequency, coherence, temperature spectral density, wave-induced spectral density, and average phase angle (between the wave and temperature spectra) at the point of maximum coherence in the wave and temperature spectra.

TABLE VII. Frequency Spectra Data

Run #	Depth (m)	Freq. (Hz)	Coherence max.	Temp. Spectral Value	W-I Temp. Spectral Value	Average Phase Difference
1	3.6	.092	.23	$.18 \times 10^{-4}$	$.41 \times 10^{-5}$	145
6	3.6	.092	.42	$.14 \times 10^{-2}$	$.59 \times 10^{-3}$	155
		.214	.44	$.39 \times 10^{-3}$	$.11 \times 10^{-3}$	155
7	9.3	.092	.40	$.62 \times 10^{-3}$	$.25 \times 10^{-3}$	140
8a	13.8	.092	.37	$.64 \times 10^{-5}$	$.24 \times 10^{-5}$	105

Figure 24 shows the measured temperature and calculated wave-induced temperature spectra, and the coherence and phase angle between waves and temperature which are discussed in the following sections.

2. Coherence

The measured coherence between waves and temperature is shown in the middle graph of Figure 24 as the solid line. The (theoretical) coherence between waves

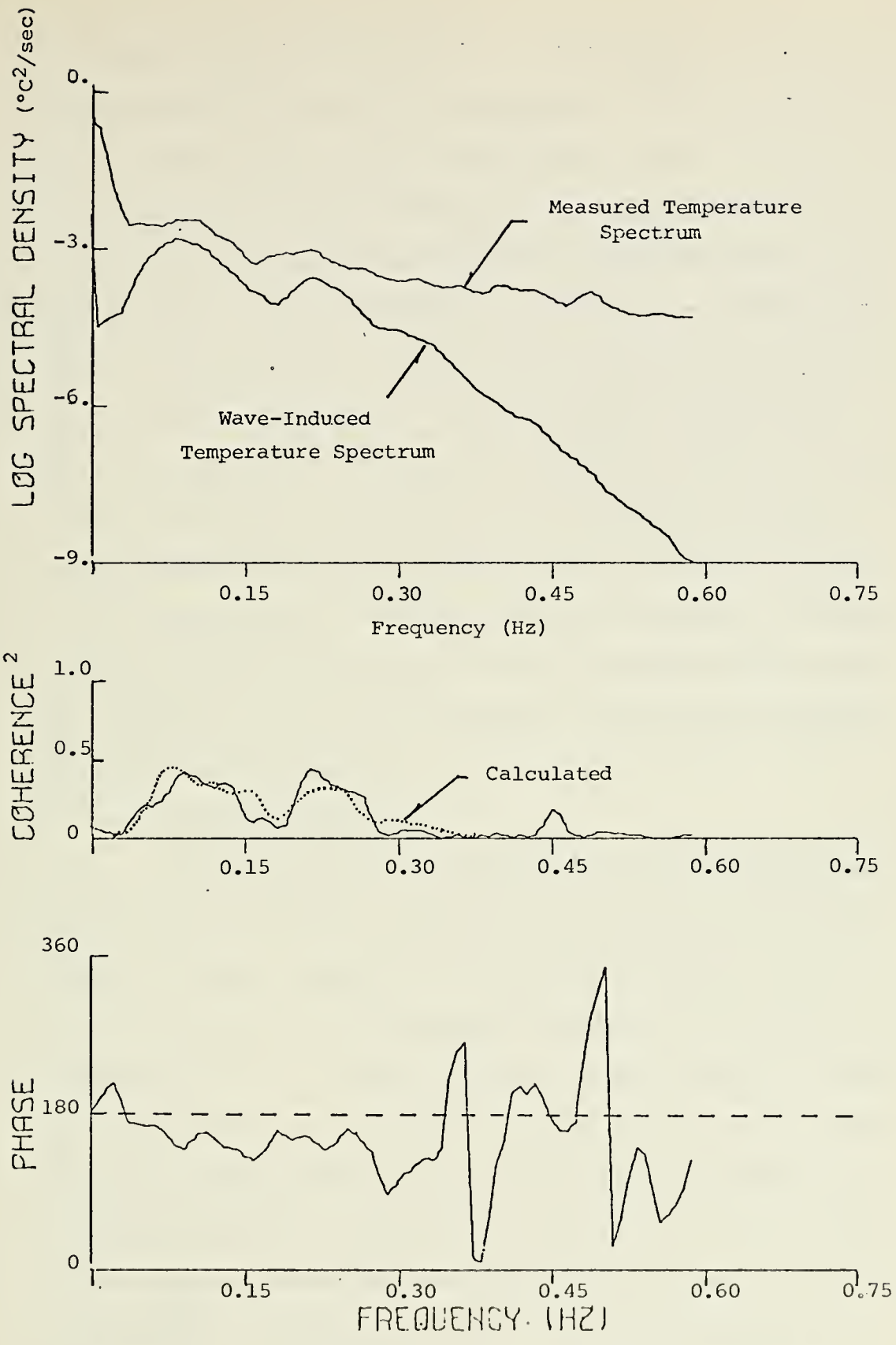

Figure 24. Actual and Calculated Wave-Induced Temperature Spectra, Run 6.

and wave-induced temperature was calculated from Equation (11) assuming statistical independence and is illustrated as the dashed line on the same figure. It is only in the relatively narrow band from 0.05 to 0.3 Hz that there is significant coherence between the spectra of waves and temperature. This corresponds to periods of between 3.3 and 20 seconds which is most certainly characteristic of surface waves and swell. The theoretical coherence, which was adjusted to match the measured coherence at the first peak value, approximates the measured coherence very closely. Hence the separation of the two spectra can be interpreted, from the increasing lack of coherence with increasing frequency, as an increasingly high ratio of turbulence (noise) to coherent surface wave-induced temperature fluctuations.

3. Phase Difference

The last graph in Figure 24 is the measured spectral phase difference between the waves and the temperature. A visual inspection of the figure reveals that over the range of significant coherency, the average phase difference is 155° (values for the other runs are listed in Table VII). In theory, the phase of the waves should lead the temperature by 180°. The difference was unexpected since the results of Thornton et al (1974) indicated a much closer relationship between theory and actual measurement. In addition they found that the span over

which the phase difference was close to 180° was much wider than the frequency band of high coherence. This occurred in these results only once, in Run 7. Also, the phase difference appeared to be depth dependent because in Runs 6 to 8a where the depth of the sensor (Thermistor 5) increased, the phase difference decreased from 155 to 105°.

The reasons for these differences are not readily forthcoming. In Run 1, as noted earlier, the stratification was different from the other runs in that over the length of the array the temperature field was highly suggestive of some double-diffusion mechanism operating. This may suggest that in such cases buoyancy plays a much greater part in the destruction of coherence between waves and temperature than in cases where temperature steadily decreases with depth.

The actual difference between the average phase difference and 180° is even more puzzling. With their sensor at 5.5 m Thornton et al (1974) found almost exactly a 180° phase difference from about .05 to 0.22 Hz. The results of this experiment at a lesser depth indicate a phase change of about 155° (about 25° difference) which decreased as the sensor depth increased. At first the difference was attributed to the horizontal displacement (leading to a phase lag) of Thermistor 5 from the Baylor Wave Gauge. The first order expressions for the wave and

temperature fluctuations are:

$$\eta = a \cos(kx - \sigma t)$$

$$\theta = H_\sigma(\theta)\, a \cos(kx - \sigma t)$$

$$= -H_\sigma(\theta)\, a \cos[180° - (kx - \sigma t)] .$$

Using the wave gauge as a reference position, the phase angles become,

$$\Sigma_\eta = -\sigma t$$

$$\Sigma_\theta = 180° - (K\Delta x - \sigma t) ,$$

so that the phase difference, $\Delta\Sigma = \Sigma_\theta - \Sigma_\eta$, is 180° if Δx is zero. The horizontal displacement was 0.19 m which for this calculation at the frequency of maximum coherence yielded a difference of 0.52° from 180°. This is a definite indication that all is not as simple as the assumptions in the model would have us believe. Internal waves, which of themselves would be 180° out of phase with the temperature fluctuations, would certainly complicate the picture because of their interaction with the surface waves and the vertical displacement of the thermistor and the wave gauge. Buoyancy effects brought about by small scale instabilities such as those noted in Run 7 may be another factor. Whatever the cause, it can be said from these results that the phase difference is not due to the surface wave-induced motions alone.

4. Turbulent Temperature Fluctuations

If in the consideration of the theory we assume that turbulent and wave-induced temperature fluctuations are statistically independent, then the area between the spectral energy density curves on Figure 24 should represent the turbulent energy as given by Equation (10). Figure 25 is a plot of the turbulent temperature spectrum for Run 6. Thornton et al (1974) calculated the turbulent temperature spectra considering the possibilities that turbulent and wave-induced temperature fluctuations were correlated (Equation (8)) as well as statistically independent (Equation (10)). They reported almost identical results. Hence, only the latter is shown here.

The turbulent spectra for all the runs were generally consistent and compared well with the -5/3 slope illustrated in Figure 25. There is a definite indication of a change over in the inertial subrange at a period of about 9 seconds (f = .11 Hz). This is to be expected since turbulence occurs at scales smaller than those associated with the waves from which turbulent energy is derived. In fact, the slope of the spectra is much nearer to -2 than -5/3. Black (1965) has suggested this slope is to be expected more often than -5/3 when there is density stratification. This would agree with the results suggested by the calculated structure function. These results appear to generally validate the assumption of statistical independence between turbulence and wave-induced

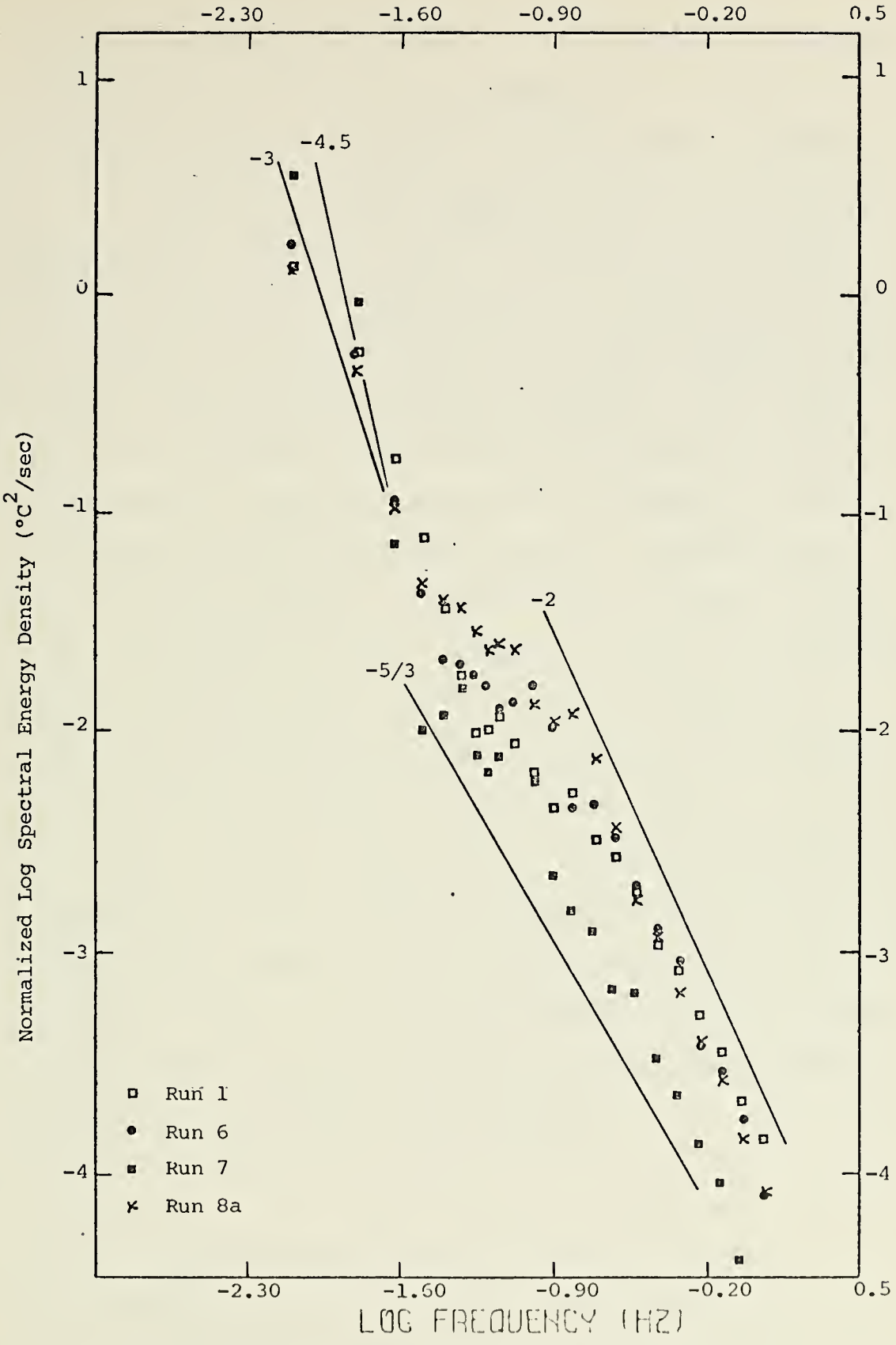

Figure 25. Turbulent Temperature Spectra.

temperature fluctuations and that the natural preference in nature is for a near -5/3 dependence of turbulent spectral energy on frequency in the inertial subrange.

Seitz (1971) has suggested that in a stationary, homogeneous, isotropic field of turbulence the energy spectra will have a dependence on a -2 power law at low frequencies and a -5/3 power law at high frequencies providing convection velocities are moderate. The transition from one power law to the other should be at some intermediate frequency and would be a function of the magnitude of the convection velocity. Following this line of reasoning then it can be seen in Figure 25 that all runs exhibit inertial subrange character in the energy spectra above 0.1 Hz. Runs 1 and 8a, which had no apparent internal wave activity, exhibit similar slopes of -7/3 below 0.031 Hz with transition between these frequencies. However, Runs 6 and 7, which did show significant internal wave activity, exhibit slopes of -3 and -4.5 respectively below 0.031 Hz. This would tend to reinforce the notion that internal waves contain much more energy at the lower frequencies and are primarily responsible for the time series being non-stationary.

V. CONCLUSIONS

The temperature field is extremely complex in the shallow waters near the NUC Tower. There were indications that double-diffusion type microstructure was present as well as the more normal, for this area, billow turbulence microstructure which appeared to be suggested by the temperature stratification for the majority of the runs.

Temperature fields with no apparent internal waves may contain turbulent oscillations suggestive of internal waves or their remnants. The basis for this statement is that the oscillations in Run 1 appeared to be periodic of period three minutes which is close to that reported by LaFond (1966) for internal waves.

Significant internal waves present on the two days of the experiment were periodic with approximately 20 minute periods. In form they were more like solitary waves rather than sinusoids but this is probably due to the fact that they were shallow water waves at this location. Judging from the temperature profiles the internal waves appeared to have positive displacement from a mean position with little or no negative displacement. The positive displacements occupied less than one-half of one period.

Internal waves appeared to be the major source of turbulence during this experiment under the conditions of

light winds and small ampitude waves. This conclusion is based on the higher variances in the runs with internal waves.

When internal waves were present there was significantly more energy at all wavenumbers and not only at low wavenumbers. This statement is predicated on the fact that even after filtering out waves of period 100 seconds and greater the runs with internal waves still had more energy than runs without internal waves.

Internal waves may possibly break, thus contributing a large amount of turbulent energy to a localized area and thus assist mixing.

With respect to spatial correlation lengths, the length of the array (64 inches = 1.6 meters) was too short to measure the scale length of the internal waves. The high-pass filtered time series had correlation lengths of 130 cm and less. There did not appear to be any depth dependence on the length but there may have been a dependence on whether the array was vertical or horizontal.

With respect to the gradient field, it is confirmed that temperature gradients taken over short distances are extremely variable over time and space as expected for a turbulent phenomenon.

Wavenumber spectra may be significantly altered at higher wavenumbers depending on the type of interpolation used in determining the spatial correlation function to be Fourier transformed. Further, the vertical and perhaps

the horizontal particle displacements at the frequency of maximum coherence in the frequency spectra appear as changes of slope in the wavenumber spectra.

The conclusions reached in respect to the spectral model proposed by Thornton et al (1974) were that:

1. The model is not always realistic in the specification of a constant mean gradient. The gradient required to be used in the transfer function to achieve consistency between the actual temperature spectrum and the wave-induced temperature spectrum was much less than the observed or calculated mean gradients.

2. The wave-induced temperature spectrum of the model showed great similarity to the actual temperature spectrum over a narrow band of frequencies associated with regions of high coherence between surface waves and temperature spectra.

3. The model describes reasonably well the wave-induced temperature fluctuations in shallow water (less than 18 m).

4. The model illustrates that moderate waves do little mixing and serve only to pump the thermocline (and temperature field) up and down.

5. The temperature field lags the wave field by approximately 180°; but the lag is modified by as yet undetermined factors and depth. The spectral analysis yielded the above with respect to surface waves and the results of the isotherm plot in Run 3 indicate the same for internal waves.

6. The model demonstrates the high probability of statistical independence between turbulent and wave-induced temperature fluctuations.

7. The turbulent temperature spectra agrees very well with inertial subrange theory in that the slopes of the log/log spectra are very near -5/3. That the slope is nearer to -2 may indicate that the time series was non-stationary.

8. The low frequency end of the turbulent spectra appears to have different slopes depending on whether the individual run had internal waves present.

LIST OF REFERENCES

1. Black, C. F., The Turbulent Distribution of Temperature in the Ocean, The Bissett-Berman Corporation, Report MJO 1049, p. 1-8, December 1965.

2. Denner, W. W., "The Layered Microstructure and Acoustic Propagation in the Arctic Ocean." U.S. Navy Journal of Underwater Acoustics, Vol. 21, No. 1, p.45-51, January 1971.

3. Gregg, M. C., "The Microstructure of the Ocean." Scientific American, Vol. 228, No. 2, p. 65-77, February 1973.

4. Gregg, M. C., Cox, C. S., and Hacker, P. W., "Vertical Microstructure Measurements in the Central North Pacific." Journal of Physical Oceanography, Vol. 3, p. 458-469, October 1973.

5. LaFond, E. C., "Internal Waves." The Encyclopedia of Oceanography, Encyclopedia of Earth Sciences Series, Vol. 1, Edited by R. W. Fairbridge, p. 402-408, Reinhold Publishing Corporation, 1966.

6. Minard, J. E., A Study of the Effect of Internal Wave Induced Turbulence on Small Scale Temeprature Structure in Shallow Water, M. S. Thesis, Naval Postgraduate School, September 1973.

7. Neshyba, S., Neal, V. T. and Denner, W. W., "Temperature and Conductivity Measurements under Ice-Island T-3." Journal of Geophysical Research, Vol. 76, No. 33, p. 8107-8120, November 1971.

8. Phillips, O. M., The Dynamics of the Upper Ocean, Cambridge University Press, 1969.

9. Chesapeake Bay Institute Technical Report 72, Results of a Field Study using the 3-Axis Doppler Shift Current Meter, by R. C. Seitz, Reference 71-6, The Johns Hopkins University, September 1971.

10. Thornton, E. B., Separating Turbulent and Wave-Induced Fluctuation: Part I, Water Parcile Velocities, Naval Postgraduate School, 1974.

11. Thornton, E. B., Boston, N.E.J., and Whittemore, M.A.N., Separating Turbulent and Wave-Induced Fluctuations: Part 2, Temperature, Naval Postgraduate School, 1974.

12. Whittemore, M.A.N., Small Scale Temperature Fluctuations near the Sea Surface, M. S. Thesis, Naval Postgraduate School, March 1973.

13. Woods, J. D., "Wave-Induced Shear Instability in the Summer Thermocline." Journal of Fluid Mechanics, Vol. 32, Part 4, p. 791-800, 1968.

14. Woods, J. D. and Wiley, R. L., "Billow Turbulence and Ocean Microstructure." Deep-Sea Research, Vol. 19, p. 87-121, Pergamon Press, 1972.

INITIAL DISTRIBUTION LIST

		No. Copies
1.	Defense Documentation Center Cameron Station Alexandria, Virginia 22314	2
2.	Library (Code 0212) Naval Postgraduate School Monterey, California 93940	2
3.	Department of Oceanography, Code 58 Naval Postgraduate School Monterey, California 93940	3
4.	Dr. E. B. Thornton, Code 58 Department of Oceanography Naval Postgraduate School Monterey, California 93940	5
5.	Dr. Noel E. Boston, Code 58 Department of Oceanography Naval Postgraduate School Monterey, California 93940	5
6.	Oceanographer of the Navy Hoffman II 200 Stovall Street Alexandria, Virginia 22332	1
7.	Naval Oceanographic Office Library (Code 3330) Washington, D. C. 20373	1
8.	Staff Officer External Affairs Defence Research Establishment Ottawa Ottawa, Ontario, Canada K1A OK2	1
9.	Staff Officer External Affairs Defence Research Establishment Pacific Esquimalt, British Columbia, Canada	1
10.	Staff Officer External Affairs Defence Research Establishment Atlantic Dartmouth, Nova Scotia, Canada	1

11. Commandant — 2
Canadian Forces Fleet School
C F B Halifax
Halifax, Nova Scotia, Canada

12. Captain J. W. Powell — 3
1072 Indian Village Road
Pebble Beach, California 93953

13. Director of Defense Research & Engineering — 1
Office of the Secretary of Defense
Washington, D. C. 20301
ATTN: Office, Assistant Director (research)

14. Office of Naval Research
Arlington, Virginia 22217
ATTN: (Code 480) — 3
ATTN: (Code 460) — 1
ATTN: (Code 102-0S) — 1
ATTN: (Code 105) — 6

15. Director
Naval Research Laboratory
Washington, D. C. 20375
ATTN: Library, Code 2620 — 6

16. Commander
Naval Oceanographic Office
Washington, D. C. 20390
ATTN: Code 1640 — 1
ATTN: Code 70 — 1

17. NODC/NOAA — 1
Rockville, Maryland 20882

18. National Defence Headquarters
Ottawa, Ontario, Canada
K1A OK2
ATTN: DGITP — 1

19. SIO Library — 1
University of California, San Diego
P. O. Box 2367
La Jolla, California 92037

20. Department of Oceanography Library — 1
University of Washington
Seattle, Washington 98105

21. Department of Oceanography Library — 1
Oregon State University
Corvalis, Oregon 97331

SECURITY CLASSIFICATION OF THIS PAGE (When Data Entered)

REPORT DOCUMENTATION PAGE

READ INSTRUCTIONS BEFORE COMPLETING FORM

1. REPORT NUMBER	2. GOVT ACCESSION NO. / 3. RECIPIENT'S CATALOG NUMBER
4. TITLE (and Subtitle): An Investigation of Surface and Internal Wave-Induced Turbulence in Shallow Water Thermal Microstructure	5. TYPE OF REPORT & PERIOD COVERED: Master's Thesis, March 1974
	6. PERFORMING ORG. REPORT NUMBER
7. AUTHOR(s): James Wesley Powell	8. CONTRACT OR GRANT NUMBER(s): Project Order No.P04-0121, ONR 55859, Research Project RR131-0301
9. PERFORMING ORGANIZATION NAME AND ADDRESS: Naval Postgraduate School, Monterey, California 93940	10. PROGRAM ELEMENT, PROJECT, TASK AREA & WORK UNIT NUMBERS: Program Element 61153N, Task NR 083-275-2
11. CONTROLLING OFFICE NAME AND ADDRESS: Naval Postgraduate School, Monterey, California 93940	12. REPORT DATE: March 1974
	13. NUMBER OF PAGES: 87
14. MONITORING AGENCY NAME & ADDRESS(if different from Controlling Office): Office of Naval Research, Arlington, Virginia 22217	15. SECURITY CLASS. (of this report): Unclassified
	15a. DECLASSIFICATION/DOWNGRADING SCHEDULE

16. DISTRIBUTION STATEMENT (of this Report)

Approved for public release, distribution unlimited.

17. DISTRIBUTION STATEMENT (of the abstract entered in Block 20, if different from Report)

18. SUPPLEMENTARY NOTES

Master of Science Thesis supervised by Dr. E. Thornton and Dr. N. Boston, Associate Professors, NPS

19. KEY WORDS (Continue on reverse side if necessary and identify by block number)

Internal Waves
Temperature Microstructure
Temperature Fluctuations
Temperature Gradients
Temporal and Spatial Spectral Analysis
Turbulent Temperature Spectra
Wave-induced Temperature Fluctuations

20. ABSTRACT (Continue on reverse side if necessary and identify by block number)

Measurements of temperature, wave height, and orthogonal water particle velocity were made in May 1973 at the NUC Tower located one mile off Mission Beach, California. A detailed analysis of the temperature field was made using digital temperature and isotherm contour plots. Billow turbulence microstructure appeared to be the dominant mechanism with the exception of one run in which evidence of double-diffusion microstructure was found. Spatial correlation lengths,

DD FORM 1 JAN 73 1473 EDITION OF 1 NOV 65 IS OBSOLETE
S/N 0102-014-6601

(Page 1)

SECURITY CLASSIFICATION OF THIS PAGE (When Data Entered)

calculated from the plot of the covariances, were of the order of 130 cm and less when the signal was high-pass filtered for waves of 100 seconds and longer. No depth dependence was noticed. Both frequency and wavenumber spectra were calculated and a correspondence between the spectra was noted at the frequency and wavenumber of the surface wave-induced particle displacements.

The Thornton, Boston, Whittemore model of wave-induced temperature fluctuations was tested and found to model the temperature spectra quite well, especially in a narrow band of frequencies associated with surface waves. The turbulent temperature spectrum, calculated as the difference between the actual and wave-induced spectra, had a slope near -5/3 above 0.1 Hz and more negative at lower frequencies.